

# Theory of free fermions dynamics under partial post-selected monitoring

Chun Y. Leung,<sup>1</sup> Dganit Meidan,<sup>2,3</sup> and Alessandro Romito<sup>1</sup>

<sup>1</sup>*Department of Physics, Lancaster University, Lancaster LA1 4YB, United Kingdom*

<sup>2</sup>*Department of Physics, Ben-Gurion University of the Negev, Beer-Sheva 84105, Israel*

<sup>3</sup>*Université Paris-Saclay, CNRS, Laboratoire de Physique des Solides, 91405, Orsay, France.*

(Dated: 25/10/2024)

Monitored quantum systems undergo Measurement-induced Phase Transitions (MiPTs) stemming from the interplay between measurements and unitary dynamics. When the detector readout is post-selected to match a given value, the dynamics is generated by a Non-Hermitian Hamiltonian with MiPTs characterized by different universal features. Here, we derive a *partial post-selected* stochastic Schrödinger equation based on a microscopic description of continuous weak measurement. This formalism connects the monitored and post-selected dynamics to a broader family of stochastic evolution. We apply the formalism to a chain of free fermions subject to partial post-selected monitoring of local fermion parities. Within a 2-replica approach, we obtained an effective bosonized Hamiltonian in the strong post-selected limit. Using a renormalization group analysis, we find that the universality of the non-Hermitian MiPT is stable against a finite (weak) amount of stochasticity. We further show that the passage to the monitored universality occurs abruptly at finite partial post-selection, which we confirm from the numerical finite size scaling of the MiPT. Our approach establishes a way to study MiPTs for arbitrary subsets of quantum trajectories and provides a potential route to tackle the experimental post-selected problem.

The field of entanglement dynamics in monitored many-body systems has recently emerged as a promising arena to explore universal collective phenomena far from equilibrium. The underpinning physics stems from generic unitary dynamics, which builds entanglement between different parts of the system, and measurements, which disentangle and localize information. The interplay between the two leads to Measurement-induced Phase Transitions (MiPTs) between phases with different entanglement scaling. MiPTs have been originally discovered in random quantum circuits [1–4]. Fueled by the experimental progress in the realization of quantum simulators, the field has then established unexpected connections with condensed matter physics, statistical mechanics, and the field of quantum information science [5], with initial evidence of MiPTs reported in recent experiments [6–8]. Quite generally, the hybrid unitary-measurement dynamics underpinning MiPT fall into 2 classes: quantum circuits with unitary gates punctuated with measurement [5], and system evolving under continuous measurements and Hamiltonian dynamics [9–33]. In both scenarios, MiPTs between phases with distinct topological quantum order from measurements-only dynamics have also been identified [10, 34–39].

Entanglement phase transitions can originate from a different kind of non-unitary dynamics generated by non-Hermitian Hamiltonians. In the simplest terms, non-Hermitian Hamiltonians describe dissipation and/or gain in a system, providing one of the simplest ways to model non-equilibrium. These models too have shown novel entanglement transitions [40–45], and transition between states with different topological order [46–51]. Notably, some non-Hermitian dynamics can be established as a limit of monitored systems when retaining a pre-determined measurement readout (full post-selection). The post-selection limit is most easily seen as the no-click

limit in the quantum jump process where one only post-selects quantum trajectories with no-click events [52], but it is a generic feature of monitored dynamics [10, 42, 53–64].

MiPTs in the post-selected limit of monitored dynamics exhibit key differences compared to their monitored counterparts. These differences extend from features of the phase diagram to the universality class of the transition [10, 53]. There have been some steps to incorporate sparse quantum jumps beyond the post-selected limit [55, 57] or to map the full crossover explored numerically [10], however, a theory that captures a systematic way to include a fraction of trajectories and explains the change in MiPTs properties is generally lacking. This is the question we address in this paper. We first summarize here our main findings.

We derive a *partial-post-selected* (PPS) *stochastic Schrödinger equation* (SSE) — cf. Eq.(9), with a continuous parameter  $\zeta \in [0, 1]$  that controls the range of detector’s outcomes that are retained. The PPS-SSE includes the fully monitored and fully post-selected dynamics as limiting cases and is valid for a generic quantum system with a continuously monitored Hermitian observable.

Next, we apply our analytic PPS approach to study the MiPT driven by non-commuting sets of local parity measurements in a real free fermionic chain. In this model, the post-selected dynamics feature an area-to-area topological MiPT driven by the competing measurements, with a different critical exponent than its monitored analogue [10]. We use the PPS-SSE approach to calculate the conditional entropy across the transition. This allows us to use a two-replica limit, for which we obtain an effective description of the steady-state out-of-equilibrium phases in terms of an effective Hamiltonian— cf. Eqs. (37,46,43). From a Renormalization Group (RG) flow analysis, we find that the post-selected universal

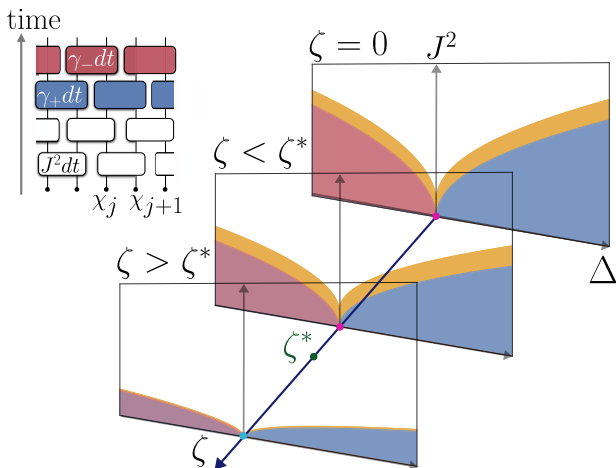


FIG. 1. Schematic drawing of the phase diagram for the model in the inset under partial post-selection. The parameter  $\zeta \in [0, 1]$  controls the degree of partial post-selection, with no postselection for  $\zeta = 1$  and complete postselection for  $\zeta = 0$ . The system displays topological trivial (blue) and non-trivial (purple) entanglement area-law phases, as well as critical log-scaling (orange) and  $\log^2$ -scaling (white) phases. The measurement-only phase transition (at  $\Delta = 0$  on the  $J^2 = 0$  line) changes its universality class with the degree of post-selection from the post-selected one (red dot) for  $\zeta < \zeta^*$  to the full monitored one (cyan dot) for  $\zeta > \zeta^*$ . Inset: quantum circuit representation of the model consisting of random Unitary evolution (white) and competing sets of Majorana fermions' bond-parity measurements of strength  $\gamma_+ = \gamma(1 + \Delta)$  (blue) and  $\gamma_- = \gamma(1 - \Delta)$  (purple)

properties of the MiPT persist when one moves away from the post-selected limit by increasing the range of outcomes retained —cf. Sec. V A, Fig. 5.

Our calculation further shows that the Luttinger parameter of the effective bosonized theory for strong post-selection diverges at a finite value of partial post-selection,  $\zeta$ , which may indicate a phase transition driven by the stochasticity from quantum trajectories. This result is supported by numerical calculation, which identifies the non-monotonic behaviour of the critical exponent at similar values of  $\zeta$  —cf. Fig. 7.

In the presence of unitary dynamics, the partial post-selected model features two distinct area law phases separated by a sub-volume law phase. We find that the sub-volume phase becomes increasingly stable upon moving away from the post-selected limit, as shown in Fig. 1 —cf. Sec. V B, Fig. 9.

The rest of the paper is structured as follows. We develop the formalism of partial post-selection in Sec. I and extend it to the replica formalism in Sec. II. Sec. IV presents the model of interest, with the corresponding effective 2-replica description in Sec. IV B and the effective theory for the strong-post-selection regime in Sec. IV C. The results are presented in Sec. V with a final discussion and conclusions in Sec. VI. Throughout this paper, we shall use the terms ‘post-selected’ and ‘monitored’ to

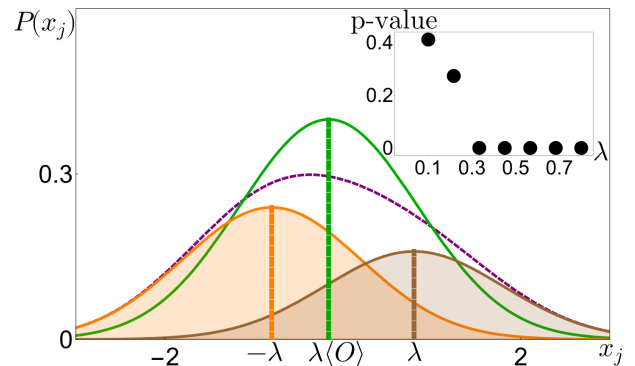


FIG. 2. Probability distribution of continuous Gaussian measurement readouts (3). The readout distribution  $P(x_j)$  (dashed purple) results from the sum of two overlapping Gaussians (brown and orange shaded), centred at positions  $\lambda$  and  $-\lambda$  with different heights  $\langle \Pi_{j,-} \rangle$  and  $\langle \Pi_{j,+} \rangle$  respectively.  $P(x_j)$  is approximated by the Gaussian distribution (green) in Eq. (3) which becomes exact in the limit of continuous measurements — cf. inset. Inset: Accuracy of the approximation in Eq.(3) quantified via a two-sample Kolmogorov-Smirnov test [65]. The accuracy (p-value) increases with decreasing  $\lambda$ , and becomes exact in the case of continuous measurement  $\lambda \sim \sqrt{dt} \rightarrow 0$ . The parameters are set as  $\lambda = 0.8$ ,  $\langle \Pi_{j,+} \rangle = 0.4$  and  $\langle \Pi_{j,-} \rangle = 0.6$ .

indicate respectively the fully post-selected measurement dynamics and the fully stochastic continuous measurement where all readouts are retained respectively.

## I. PARTIAL POST-SELECTION

We consider the dynamics of a continuously monitored quantum system whose evolution is described by the stochastic Schrödinger equation (SSE)

$$d|\psi_t\rangle = \left[ -idtH - dt\frac{\gamma}{2} \sum_j (\hat{O}_j - \langle \hat{O}_j \rangle)^2 + \sum_j dW_j (\hat{O}_j - \langle \hat{O}_j \rangle) \right] |\psi_t\rangle, \quad (1)$$

where  $|\psi_t\rangle$  is the system's state at time  $t$ ,  $\hat{O}_j$  the set of observables being measured, and  $H$  the system's Hamiltonian. To lighten the notation, we shall drop the hat above the measurement operator unless it is needed for clarity. Eq.(1) is the Ito formulation of stochastic dynamics with  $dW_j$  uncorrelated Gaussian-distributed stochastic increments with  $\overline{dW_j dW_k} = \gamma dt \delta_{j,k}$ , where  $\gamma$  is the inverse measurement time at which typical stochastic realizations of the quantum trajectories are close to the observable's eigenvalue.

To develop the idea of partial post-selection, we start with a microscopic model of the measurement process leading to the SSE. We consider the measure-

ment process described by a positively valued measurement [52]. In this case, after coupling the detector to the system in a state  $|\psi\rangle_t$ , the process returns a readout  $x_j$ , drawn from a probability distribution  $P(x_j) = \langle \psi_t | K_j(x_j)^\dagger K_j(x_j) | \psi_t \rangle$ , and a conditional state update  $|\psi_{t+dt}\rangle = K_j(x_j) |\psi_t\rangle / \sqrt{P(x_j)}$ . The process is entirely dictated by the Kraus operators  $K_j(x_j)$ .

We consider here specifically the case of continuously monitoring an observable  $O_j$  as performed by a pointer with a continuous readout  $x_j$  with Gaussian a-priori distribution  $G(x) = 1/\sqrt{2\pi\Delta^2} \exp(-x^2/2\Delta^2)$ . We further restrict to the simplest case of a measurement operator  $\hat{O}_j = \hat{\Pi}_{j,+} - \hat{\Pi}_{j,-}$  which acts in the 2-dimensional space with projector  $\hat{\Pi}_{+/-}$  and squares to identity  $\hat{O}_j^2 = \mathbb{I}$ . The Kraus operators are then given by [52]

$$K_j(x_j, \lambda) = \sqrt{G(x_j - \lambda)} \hat{\Pi}_{j,+} + \sqrt{G(x_j + \lambda)} \hat{\Pi}_{j,-}, \quad (2)$$

and

$$P(x_j) = G(x - \lambda) \langle \hat{\Pi}_{j,+} \rangle + G(x + \lambda) \langle \hat{\Pi}_{j,-} \rangle. \quad (3)$$

The continuous SSE in Eq.(1) is recovered by setting  $\lambda^2 = \gamma dt$ , where  $dt \rightarrow 0$  with  $\gamma$  finite guarantees  $\lambda \ll 1$ . In this limit,

$$P(x_j) \approx \frac{1}{\sqrt{2\pi\Delta^2}} \exp\left(-\frac{(x_j - \lambda\langle O_j \rangle)^2}{2\Delta^2}\right),$$

$$K_j(x_j, \lambda) \approx \frac{1}{(2\pi\Delta^2)^{1/4}} \exp\left(-\frac{(x_j - \lambda O_j)^2}{4\Delta^2}\right). \quad (4)$$

The probability distribution is schematically shown in Fig. 2. Notably, in Eq.(4), we have used the fact that in the continuum limit  $\lambda^2 = \gamma dt \rightarrow 0$ ,  $\Delta \sim \mathcal{O}(dt^0)$ .

The scenario of multiple measurement events can be written readily down: if there are  $L$  lots of measurement operators  $\hat{O}_j, j \in [1 \dots L]$ , the final state after measurements across all operators is

$$|\psi_{t+dt}\rangle = \frac{1}{\mathcal{N}} \prod_{j=1}^L K_j(x_j, \lambda) |\psi_t\rangle, \quad (5)$$

where the results hold in the continuum limit  $dt \rightarrow 0$  to order  $\mathcal{O}(dt)$  also if some of the operators  $O_j$  do not commute. As a side note, (2) can also be generalised to measurement operators with arbitrary spectrum with the same procedure illustrated above [52].

The process of post-selection amounts to choosing and retaining the quantum trajectories that correspond to a unique set of predetermined detector readouts  $\{x_j\}$ , while discarding the rest. We generalize this procedure to achieve Partial Post-Selection (PPS) by retaining all quantum trajectories that correspond to a finite range of detector outcomes. A natural means to achieve PPS is to force some degree of bias in the measurement outcome retaining the detector's outcome only if they are larger

than a given, preset value,  $r_c$ . This amounts to truncating the readout probability distribution function  $P(x_j)$  to a modified one,

$$P_{r_c}(x_j) = P(x_j) \Theta(x_j - r_c) \approx e^{-\frac{(x_j - \lambda\langle O_j \rangle - \delta\lambda)^2}{2(\Delta + \delta)^2}} \equiv \underline{P}(x_j), \quad (6)$$

where  $\Theta(x)$  is the Heaviside step function.

In the last step in Eq.(6), we have approximated the truncated distribution by a new Gaussian distribution whose mean and variance are shifted w.r.t. the original Gaussian  $P(x_j)$ , parametrised by  $\delta\lambda$  and  $\delta$  respectively, are determined by demanding that they coincide with those of  $P_{r_c}(x_j)$ , as illustrated in Fig. 3. While the distribution  $P_{r_c}$  and  $\underline{P}$  are generically different, we demand a proper scaling of  $r_c$  with  $dt \rightarrow 0$  so that the two distributions coincide in the continuum limit. This is achieved with the scaling

$$\delta\lambda = \frac{(1 - \zeta)}{\zeta} \lambda = \frac{(1 - \zeta)}{\zeta} \sqrt{\gamma dt}, \quad (7)$$

where we have introduced a dimensionless parameter  $\zeta \in [0, 1]$  which controls the degree of partial post-selection, and  $\zeta$  is kept constant in the limit  $dt \rightarrow 0$  (see Appendix A). The relation between  $r_c$  and  $\zeta$  is derived and discussed in Appendix A, and  $\zeta$  captures the discrete-time partial post-selecting process  $r_c$  in the time continuum limit, in analogy to the continuous measurement strength  $\gamma$  capturing the discrete-time strength  $\lambda$  for continuous measurement backaction. On the other hand, the correction in variance,  $\delta$ , can be safely ignored (Appendix A). Importantly, at leading order in  $dt$ , the functional dependence of  $\zeta$  on  $r_c$  is independent of the system's state so that the continuum limit at constant  $\zeta$  corresponds to an operationally well-defined truncation of the probability  $P(x_j)$ .

We show explicitly via a two-sample Kolmogorov-Smirnov (KS2) test from a numerical sampling of  $P_{r_c}(x_j)$  and  $\underline{P}(x_j)$  [65], that the approximation by a Gaussian distribution in the time continuum analysis becomes exact in the continuum limit. The results are reported in figure 3, with the inset showing that the p-values (a statistical measure of overlap) of the two distributions are increasing with small time increments  $dt$ .

The continuum limit of  $\underline{P}(x_j)$  in Eq.(6), allows us to obtain a corresponding PPS SSE. Specifically, we introduce a new random variable  $\Delta\xi_j = x_j - \lambda\langle O_j \rangle - \delta\lambda$ , with  $\mathbf{mean}(\xi_j) = 0$  and  $\mathbf{Var}(\xi_j) = 1$ . When expressed in terms of  $\xi$ , the update of the state by the Kraus operator in (5) becomes

$$\begin{aligned} |\psi_{t+dt}\rangle &= \frac{1}{\mathcal{N}} \prod_j K_j(x_j, \lambda) |\psi_t\rangle \\ &= \frac{1}{\mathcal{N}_2} \prod_j e^{\left(\frac{\lambda^2(O_j - \langle O_j \rangle - \delta\lambda)^2}{4\Delta^2} + \xi_j \lambda \frac{O_j - \langle O_j \rangle - \delta\lambda}{2\Delta}\right)} |\psi_t\rangle, \end{aligned} \quad (8)$$

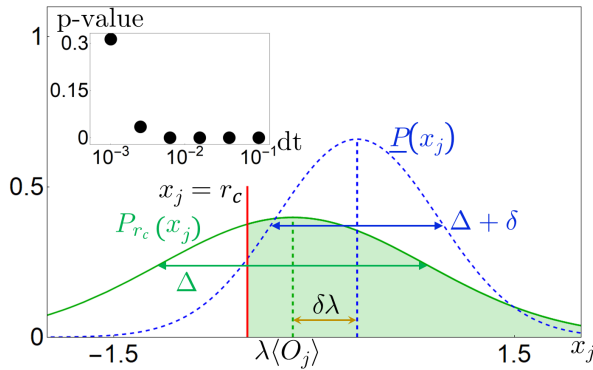


FIG. 3. Partial-post selection procedure in (6). The measurement outcome Gaussian distribution (green) is truncated at  $x_j = r_c$ , resulting in a new distribution  $P_{r_c}(x_j)$  (shaded) with shifted mean  $\lambda \rightarrow \lambda + \delta\lambda$  and shifted variance  $\Delta^2 \rightarrow (\Delta + \delta)^2$ .  $P_{r_c}$  is approximated by a new Gaussian,  $\underline{P}(x_j)$  (blue), with mean  $\lambda + \delta\lambda$  and variance  $(\Delta + \delta)^2$ . The approximation is valid in the continuum limit as shown in the inset. Inset: p-value from a KS2 test for the two distributions  $P_{r_c}$  and  $\underline{P}$  with various  $dt$ . The approximation is exact in the continuum limit  $dt \rightarrow 0$ . The parameters are set as  $\langle O_j \rangle = 0.2$ ,  $r_c = -0.5$  and  $\lambda = 0.3$ .

where overall factors have been reabsorbed in the state-normalization  $\mathcal{N}_2$ . The state update in Eq.(8) defines a Wiener process to order  $dt$ , and upon expanding up to  $\mathcal{O}(dt)$ , we arrive at the modified partial-post selected stochastic Schrödinger equation (PPS SSE)

$$\begin{aligned}
 d|\psi_t\rangle &= -idtH'|\psi_t\rangle - \frac{\zeta\gamma dt}{2} \sum_j \left(\hat{O}_j - \langle \hat{O}_j \rangle\right)^2 |\psi_t\rangle \\
 &+ (1 - \zeta)\gamma dt \sum_j \left(\hat{O}_j - \langle \hat{O}_j \rangle\right) |\psi_t\rangle \\
 &+ \sum_j dW_j \left(\hat{O}_j - \langle \hat{O}_j \rangle\right) |\psi_t\rangle, \quad (9)
 \end{aligned}$$

To obtain Eq. (9) from eq. (8) we have set  $\Delta = 1/2$  and  $\lambda^2 = \gamma dt$ , and introduced the random variable  $dW_j = \xi_j \sqrt{\gamma dt}$  with zero mean and variance  $dW_j dW_k = \zeta \gamma dt \delta_{j,k}$ . We have also rescaled the Hamiltonian via  $\zeta H = H'$  keeping  $H'$  constant. This procedure correctly accounts for the fully post-selected  $\zeta \rightarrow 0$  limit. For clarity, we hereafter identify  $H' = H$ .

Eq.(9) is the first main result of our work. It generalises the SSE to account for a partial selection of trajectories defined in an operationally meaningful procedure. From Eq.(9), we can identify two limits: for  $\zeta = 1$ , we recover the standard SSE for monitored dynamics, while for  $\zeta \rightarrow 0$ , we approach the post-selected limit governed by a non-Hermitian Hamiltonian  $H_{\text{eff}} = H + i\gamma \sum_j \hat{O}_j$ . In the following, we measure all energy scales in units of  $\gamma$ , hence set  $\gamma = 1$ .

## II. MEASUREMENT INDUCED TRANSITION AND REPLICATED DYNAMICS

The effect of partial post-selection can equivalently be captured in the evolution of the system density matrix. The density matrix evolved along a quantum trajectory with a certain set of measurement outcomes  $\{x_t\}$  at discrete times  $t \in [1 \dots M]$ , is given by

$$\rho_{\{x_t\}} = \frac{\check{\rho}_{\{x_t\}}}{\text{Tr}[\check{\rho}_{\{x_t\}}]}, \quad (10)$$

where  $\check{\rho}_{\{x_t\}} = K_{x_M} \dots K_{x_2} K_{x_1} \rho_0 K_{x_1}^\dagger K_{x_2}^\dagger \dots K_{x_M}^\dagger$  is the *un-normalised* density matrix along the trajectory,  $K_{x_t}$  the Kraus operator in Eq.(2) is associated with measurement outcome  $x_t$  and  $\rho_0$  is the initial *normalised* density matrix. From here onward, we will specify an un-normalised density matrix by a caron (reverse hat) above:  $\rho = \check{\rho} / \text{Tr}[\check{\rho}]$ .

The probability of this trajectory, labelled by  $\{x_t\}$ , is  $P(\{x_t\}) = \text{Tr}[\check{\rho}_{\{x_t\}}]$ , and the average density matrix over all trajectories is

$$\bar{\rho} = \sum_{\{x_t\}} \frac{\check{\rho}_{\{x_t\}}}{\text{Tr}[\check{\rho}_{\{x_t\}}]} P(\{x_t\}) = \sum_{\{x_t\}} \check{\rho}_{\{x_t\}}, \quad (11)$$

where we use  $\bar{\cdot}$  to indicate the average over quantum trajectories, and the sum runs over all possible sets of measurement outcomes. In the continuum limit, the evolution of  $\bar{\rho}$  is governed by a Lindblad equation, which, in the typical cases of incompatible measurements and/or unitary dynamics considered here, admits as a long-term fixed point the maximally mixed state  $\lim_{t \rightarrow \infty} \bar{\rho}_t \sim \mathbb{I}$ .

To capture non-trivial effects from measurements in the steady-state ensemble of quantum trajectories, one therefore needs to consider the evolution along individual trajectories, i.e. via post-selection, or resort to averages of quantities which are non-linear in density matrix e.g.  $\overline{\langle \hat{O} \rangle^k} = \overline{\text{Tr}[\hat{O}\rho]^k}$ . In particular, measurement-induced transitions can be tracked using quantum information quantifiers such as the  $k$ -th Renyi entropy  $\overline{S_k} = 1/(1-k) \log(\text{Tr}[\rho_{\mathbf{A}}^k]) = 1/(1-k) \log \mu_{k,\mathbf{A}}$ , for  $k > 1$ . Here  $\rho_{\mathbf{A}}$  and  $\mu_{k,\mathbf{A}} = \text{Tr}[\rho_{\mathbf{A}}^k]$  are the reduced density matrix and the  $k$ -th purity of a subsystem  $\mathbf{A}$ .

To treat analytically these non-linear averages, one can resort to a powerful mathematical construction, the replica trick [9, 18, 66, 67], where one considers identical replicas of the system's density matrix. The average of the replicated density matrix can then be related to the average of the non-linear quantities we are interested in.

In fact,

$$\begin{aligned} \overline{\langle O \rangle^k} &= \sum_{\{x_t\}} (\text{Tr}[O\rho_{\{x_t\}}])^k P(\{x_t\}) \\ &= \sum_{\{x_t\}} \text{Tr}[O^{\otimes k} \check{\rho}_{\{x_t\}}^{\otimes k}] (\text{Tr}[\check{\rho}_{\{x_t\}}])^{1-k} \\ &= \lim_{n \rightarrow 1} \sum_{\{x_t\}} \text{Tr} \left[ (O^{\otimes k} \otimes \mathbb{I}^{\otimes n-k}) \check{\rho}_{\{x_t\}}^{\otimes n} \right], \end{aligned} \quad (12)$$

and the non-linear quantity encoding the non-trivial effects of measurement-induced dynamics is the trajectories averaged  $n$ -replicated un-normalised density matrix  $\sum_{\{x_t\}} \check{\rho}_{\{x_t\}}^{\otimes n} = \overline{\check{\rho}^{\otimes n}}$ ,  $n \geq k$ . Eq.(12) shows that the fundamental object of interest is  $\overline{\check{\rho}^{\otimes n}}$ , and the limit  $n \rightarrow 1$  is an analytical continuation for  $k > 1$ . Notably, the replica limit  $n \rightarrow 1$  poses a different case from the standard limit  $n \rightarrow 0$  resulting from the replica trick for disordered systems [68, 69].

Since the  $k$ -th purity involves the  $k$ -th power of the reduced density matrix, it is the most suitable quantity to address MiPTs via the replica formalism. It can be incorporated therein by introducing an operator in the replica space,  $\mathcal{C}_{k,\mathbf{A}}$  [18, 66]

$$\mu_{k,\mathbf{A}} = \text{Tr}[\rho_{\mathbf{A}}^k] = \text{Tr}[\mathcal{C}_{k,\mathbf{A}} \rho^{\otimes k}], \quad (13)$$

where  $\rho$  is the *normalised* density matrix and

$$\mathcal{C}_{k,\mathbf{A}} = \sum_{\mathbf{A}_j} \bigotimes_{j=1}^{j=k} |\mathbf{A}_j\rangle \langle \mathbf{A}_{j+1}|, \quad (14)$$

where the sum indicates that  $|\mathbf{A}_j\rangle$  ( $j \bmod k$ ) runs over all the basis in subsystem  $\mathbf{A}$ . Note that  $\mathcal{C}_{k,\mathbf{A}}$  acts as an identity outside of  $\mathbf{A}$  while cyclically translates kets from different replica in region  $\mathbf{A}$ .

### A. Conditional purity

In the remainder of the paper, we focus on the analytical investigation of the simplest non-linear physical indicator of MiPTs in the density matrix: conditional purity. This quantity, which we denote by a double over line above,  $\overline{\overline{\mu}}_{2,\mathbf{A}}$ , was introduced in Ref. [66, 67] and is associated with the conditional 2-nd Rényi entropy  $S_{2,\mathbf{A}}^{(\text{cond})}$  as

$$\begin{aligned} \overline{\overline{\mu}}_{k,\mathbf{A}} \Big|_{k=2} &\equiv e^{-S_{k,\mathbf{A}}^{(\text{cond})}} \Big|_{k=2} \\ &= \left( \frac{\text{Tr}[\mathcal{C}_{2,\mathbf{A}} \sum_{\{x_t\}} \check{\rho}_{\{x_t\}}^{\otimes k}]}{\text{Tr}[\sum_{\{x_t\}} \check{\rho}_{\{x_t\}}^{\otimes k}]} \right) \Big|_{k=2} \\ &= \left( \frac{\sum_{\{x_t\}} P(\{x_t\})^k \text{Tr}[\rho_{\mathbf{A},\{x_t\}}^k]}{\sum_{\{x_t\}} P(\{x_t\})^k} \right) \Big|_{k=2} \\ &= \frac{\text{Tr} \rho_{\mathbf{A},M}^2}{\text{Tr} \rho_M^2}. \end{aligned} \quad (15)$$

Here,  $\rho_M$  is the reduced density matrix of the measurement devices (the ancillae) and  $\rho_{\mathbf{A},M}$  is the reduced density of subsystem  $\mathbf{A}$  along with the ancillae, where now the average over trajectories is implicitly included in the trace operation. In the measurement outcome basis, they are written as

$$\begin{aligned} \rho_M &= \sum_{\{x_t\}} \text{Tr}[\check{\rho}_{M,\{x_t\}}] |\{x_t\}\rangle \langle \{x_t\}| \\ \rho_{\mathbf{A},M} &= \sum_{\{x_t\}} \text{Tr}[\check{\rho}_{\mathbf{A},M,\{x_t\}}]_M |\{x_t\}\rangle \langle \{x_t\}|, \end{aligned} \quad (16)$$

where the trace  $\text{Tr}[\dots]_M$  denotes the partial trace w.r.t. the measurement devices.  $\rho_{\dots,\{x_t\}}$  indicates a density matrix conditional to the readouts  $\{x_t\}$  in the measurement devices. We also used the relationship  $P(\{x_t\}) = \text{Tr}[\check{\rho}_{M,\{x_t\}}]$  and the decomposition  $\check{\rho}_{\mathbf{A},M,\{x_t\}} = \check{\rho}_{\mathbf{A},\{x_t\}} \otimes \check{\rho}_{M,\{x_t\}}$ . Eq.(15) shows that  $S_{2,\mathbf{A}}^{(\text{cond})}$  is related to the 2-nd Rényi entropy of the extended system (with the ancillae), albeit shifted by a normalisation factor.

We note that the conditional purity  $\overline{\overline{\mu}}_{2,\mathbf{A}}$  in Eq.(15) differs from the subsystem purity averaged over the measurement ensemble  $\overline{\mu}_{2,\mathbf{A}}$ , but is instead calculable as the  $n = 2$ -replica limit of the latter, i.e.  $k, n = 2$  in Eq.(12). This amounts to averaging with a *distorted* probability distribution, now given by  $P(\{x_t\})^2$  as shown in Eq.(15). Nonetheless,  $\overline{\overline{\mu}}_{2,\mathbf{A}}$  corresponds to a physically well defined quantity and captures the non-linear effect of monitoring, thus providing a valid figure of merit to identify the non-trivial effects of PPS on measurement-induced dynamics [66, 67].

Finally, we caution the reader that the conditional 2-nd Rényi entropy  $S_{2,\mathbf{A}}^{(\text{cond})}$  may scale quantitatively differently from the entanglement entropy, as shown for free fermions and monitored spin-1/2 system [18, 33]. Hence, the results of our analytical theory for the observable  $S_{2,\mathbf{A}}^{(\text{cond})}$  cannot be directly extended to the Rényi entropies and entanglement entropy, but can be a valid indicator based on numerical simulations in some cases [66] (see also Sec. V).

### B. Replica dynamics in PPS

In the case of continuous measurements we are considering here, the equivalent of Eq.(9) for the density matrix along the individual trajectory is given by the stochastic

differential equation

$$\begin{aligned} \partial_t \rho = & -i \left[ \left( H + i(1-\zeta) \sum_j \hat{O}_j - \langle \hat{O}_j \rangle \right) \rho \right. \\ & \left. - \rho \left( H - i(1-\zeta) \sum_j \hat{O}_j - \langle \hat{O}_j \rangle \right) \right] \\ & - \frac{\zeta}{2} \sum_j \left[ \hat{O}_j, [\hat{O}_j, \rho] \right] + \sum_j dW_j \left\{ \hat{O}_j - \langle \hat{O}_j \rangle, \rho \right\}. \end{aligned} \quad (17)$$

Eq.(17) contains non-linear state-dependent terms. This can be circumvented using the replica trick by studying trajectory averages of the un-normalized density matrix [18]. For the class of measurement operators relevant to our problem so that  $\hat{O}^2 \propto \hat{O}$  (equivalently, there exists an associated operator  $\hat{O}' = \mathbb{I} - 2c^{-1}\hat{O}$  satisfying  $\hat{O}'^2 = \mathbb{I}$ ), the problem reduces to an average over random non-Hermitian Gaussian noise. Explicitly, we can rewrite the quantum trajectories average of an operator  $\hat{O}$  in (12) as

$$\int_{\mathcal{A}_j(t_l)} \prod_{l=1}^M \mu(\mathcal{A}_j(t_l)) \text{Tr}[\hat{O} \check{\rho}_{\mathcal{A}_j(t_l)}^{\otimes n}] = \text{Tr}[\hat{O} \mathbb{E}_G[\check{\rho}_{\mathcal{A}_j(t_l)}^{\otimes n}]] \quad (18)$$

and the notation  $\mathbb{E}_G[\dots]$  indicates a Gaussian average over all random variables  $\mathcal{A}_l$ . In the monitored dynamics, the Gaussian measure  $\mu(\mathcal{A}_j(t))$  has mean centred at  $\mathbb{E}_G[\mathcal{A}_j(t)] = 0$  and variance  $\mathbb{E}_G[\mathcal{A}_j(t)\mathcal{A}_{j'}(t')] = \gamma\delta(t-t')\delta_{j,j'}$  in time continuum. The details of the derivation are summarised in Appendix B, where we follow the notation by Ref. 18, making an explicit link to the Kraus operator introduced in Eq.(4). The result is a random non-Hermitian Hamiltonian acting on the *un-normalised* density matrix, see Eq.(B.9). The generalization to more than one set of measurements is straightforward, and here we abuse the notation  $\mathbb{E}_G[\dots]$  to denote the Gaussian average over all random variables from all measurement processes, each with its Gaussian measure.

This ‘non-Hermitian noise’ formalism can be applied to the partial post-selection procedure in Sec. I, formulated in terms of Gaussian distributed measurement readouts. As shown in Eq.(6), the overall effect of PPS is shifting the centre of the measurement readouts by an amount  $\delta\lambda = (1-\zeta)\lambda/\zeta$ . When taking the continuum limit  $dt \rightarrow 0$ , the averages of the stochastic processes in PPS SSE are equivalently described in the ‘non-Hermitian noise’ formalism by a Gaussian distribution with a shifted mean in the measure  $\mu(\mathcal{A}_j(t))$  (see Appendix B for the detailed derivation)

$$\begin{aligned} \mathbb{E}_G^{(PPS)}[\mathcal{A}_j] &= 1 - \zeta, \\ \mathbb{E}_G^{(PPS)}[\mathcal{A}_j\mathcal{A}_k] &= \zeta\delta(t-t')\delta_{j,k} + (1-\zeta)^2. \end{aligned} \quad (19)$$

This procedure can be extended further to deal with replica formalism averages. The fundamental object of interest in the replica dynamics (cf. Eq.(12)) is  $\mathbb{E}_G[\check{\rho}^{\otimes n}]$ . We will show in Sec.IV B that this will lead to an extra deterministic non-Hermitian term in the PPS dynamics.

As demonstrated in Appendix B, for the class of operators  $O^2 \propto O$ , the evolution of the unnormalized density matrix, Eq.(18), is governed by a time-dependent Hamiltonian of the form

$$H(t) = H_0 + i \sum_j \mathcal{A}_j(t) O_j. \quad (20)$$

$H_0$  represents the unitary part of the evolution and the non-unitary update from measurements is represented by the non-Hermitian contribution.

Under such mapping, the evolution of the un-normalised density matrix  $\check{\rho}(t)$ , is given by Eq.(10), which, in the time-continuous limit considered here reduces to

$$\begin{aligned} K(t) &= \exp \left[ -i \int_0^t dt' H(t') \right] \\ \check{\rho}_M(t) &= K(t)\rho(0)K^\dagger(t), \quad \rho_M(t) = \frac{\check{\rho}_M(t)}{\text{Tr}[\check{\rho}_M(t)]}, \end{aligned} \quad (21)$$

and we label the set of trajectories by  $M$ , the set of random measurement outcomes (see Appendix B for this time continuum process).

*a. Operator-to-state* —To proceed further, it is advantageous to employ the standard Choi–Jamiołkowski isomorphism to map operators into states, which we summarise in Appendix C [70, 71]. In this formalism, we can express the  $n$ -replicated density matrix (an operator in  $n$ -replicated Hilbert space) as a state in a  $2n$  duplicated Hilbert space. The evolution operator then acts as a superoperator on the duplicated Hilbert space.

$$\check{\rho}^{\otimes n}(t) \xrightarrow{\text{Choi}} |\check{\rho}^{\otimes n}(t)\rangle\rangle = (K(t) \otimes K^*(t))^{\otimes n} |\rho^{\otimes n}(0)\rangle\rangle \quad (22)$$

where the object  $|\dots\rangle\rangle$  indicates that the state lives in the duplicated Hilbert space. The details of the isomorphism and the derivation of Eq.(22) are summarised in appendix C. In this operator-to-state formalism, the trajectory-averaged  $n$ -replicated un-normalised density matrix is given by

$$\begin{aligned} \mathbb{E}_G[|\check{\rho}^{\otimes n}(t)\rangle\rangle] &\equiv |\check{\rho}^{(n)}(t)\rangle\rangle \\ &= \mathbb{E}_G[(K(t) \otimes K^*(t))^{\otimes n} |\rho^{(n)}(0)\rangle\rangle], \end{aligned} \quad (23)$$

and we shorthand  $|\check{\rho}^{(n)}(t)\rangle\rangle$  for the average un-normalised  $n$ -replicated density matrix in the duplicated Hilbert space. In particular, under Choi–Jamiołkowski isomorphism, the trace operation in Eq.(12) becomes a transition amplitude

$$\lim_{n \rightarrow 1} \text{Tr} [O^{\otimes k} \otimes \mathbb{I}^{\otimes n-k} \mathbb{E}_G[\check{\rho}^{\otimes n}(t)]] = \lim_{n \rightarrow 1} \langle\langle \mathcal{O}_k | \check{\rho}^{(n)}(t) \rangle\rangle, \quad (24)$$

where the boundary bra in the duplicated Hilbert is

$$|\mathcal{O}_k\rangle\rangle = (O \otimes \mathbb{I})^{\otimes k} \otimes (\mathbb{I} \otimes \mathbb{I})^{\otimes n-k} |\mathbb{I}\rangle\rangle. \quad (25)$$

$|\mathbb{I}\rangle\rangle$  corresponds to the identity operator in the duplicated Hilbert space.

In the 2-replica analysis of interest, the relevant conditional 2nd Rényi entropy, under operator-to-state mapping, is written as

$$e^{-S_{2,\mathbf{A}}^{(cond)}} = \bar{\mu}_{2,\mathbf{A}} = \frac{\langle\langle \mathcal{C}_{2,\mathbf{A}} |\check{\rho}^{(2)}(t) \rangle\rangle}{\langle\langle \mathbb{I} |\check{\rho}^{(2)}(t) \rangle\rangle}. \quad (26)$$

Eq.(24) shows that the averaged replicated dynamics is directly reflected by the state  $|\check{\rho}^{(n)}(t)\rangle\rangle$ , and in particular, its steady-state properties. Thus, the identification and characterization of MiPT is equivalent to the study of  $|\check{\rho}^{(n)}(t)\rangle\rangle$  in the steady-state dynamics.

### III. MONITORED DOUBLE-WELL

As a first application of the partial post-selected SSE introduced in Eq. (9), we consider a number-conserving toy model consisting of a single particle in a double well potential, in which we monitor the local occupation number. We model the system as a two-level system spanned by  $|01\rangle$  and  $|10\rangle$ , where the first (second) index is the occupation of site 1 (site 2). The unitary dynamics is governed by a tunnelling Hamiltonian  $H = -iJ|01\rangle\langle 10| + h.c.$ , and we continuously monitor the difference in the occupation number  $n_- = |01\rangle\langle 01| - |10\rangle\langle 10|$  [72]. Since the fermionic Hilbert space is 2-dimensional, we can equivalently write the dynamics in terms of a single spin 1/2 system. We identify  $|0,1\rangle$  with  $|\uparrow\rangle$  and  $|1,0\rangle$  with  $|\downarrow\rangle$ , and the PPS SSE describing the dynamics is

$$\begin{aligned} d|\psi_t\rangle &= -iJ\sigma_y dt + (1-\zeta)dt(\sigma_z - \langle\sigma_z\rangle)|\psi_t\rangle \\ &\quad - \frac{\zeta dt}{2}(\sigma_z - \langle\sigma_z\rangle)^2 |\psi_t\rangle + dW_t(\sigma_z - \langle\sigma_z\rangle)|\psi_t\rangle, \end{aligned} \quad (27)$$

where  $\overline{dW_t dW_{t'}} = \zeta \delta_{t,t'} dt$ . In the absence of partial post-selection, the physics of the model is that of the Zeno effect for continuously monitored systems [73–79]. While for the *average state*, the long-time stationary state is independent of the measurement strength; it has been shown in different measurement models that the post-selected dynamics and the *probability distribution* of steady states show distinct features in the Zeno and non-Zeno regimes [73]. To capture the effect of partial post-selection on these features beyond the average dynamics, we analyze the conditional 2-nd partial purity in Eq. (15) for a single particle where the sub-region  $\mathbf{A}$  consists of a single site:

$$\bar{\mu}_{2,\mathbf{A}} = \frac{1}{2} \left( 1 + \overline{\langle\sigma_z\rangle^2} \right). \quad (28)$$

We can, therefore, use the formalism developed in Sec. II. As pointed out in Sec. IIB, the non-linear dynamics at hand can be reformulated into a simpler Gaussian averaging problem ( $\sigma_z^2 = \mathbb{I}$ ). Under the Wiener-to-non-Hermitian mapping, the relevant Hamiltonian to our problem is

$$H(t) = J\sigma_y + iM_1(t)\sigma_z, \quad (29)$$

and  $M_1(t)$  is a Gaussian stochastic variable whose mean and variance are (cf Eq.(19)):  $\mathbb{E}_G[M_1(t)] = 1 - \zeta$ ,  $\mathbb{E}_G[M_1(t)M_1(t')] = \zeta\delta(t-t') - (1-\zeta)^2$ . The Kraus operator governing the evolution of the density matrix follows directly from Eq.(21).

Utilising the operator-to-state mapping, we can compute  $\bar{\mu}_{2,\mathbf{A}}$  via Eq. (26) and Eq.(22) with  $n = 2$ , where the ket in the duplicated Hilbert space has dimension 16. The Gaussian average can be evaluated utilising a cumulant expansion up to the second order (see later part of Appendix C), resulting in the following *deterministic* effective Hamiltonian in the 2-replica dynamics:

$$\begin{aligned} |\check{\rho}^{(2)}(t)\rangle\rangle &= e^{-itH_{\text{eff}}} |\check{\rho}^{(2)}(0)\rangle\rangle \\ H_{\text{eff}} &= \sum_{\substack{\sigma=\pm \\ a=1,2}} \left[ J\sigma_y^{(\sigma a)} + i(1-\zeta)\sigma_z^{(\sigma a)} \right] + i\zeta \left( \sum_{\substack{\sigma=\pm \\ a=1,2}} \sigma_z^{(\sigma a)} \right)^2. \end{aligned} \quad (30)$$

The choice of the initial state is unimportant, and  $\lim_{t \rightarrow \infty} |\check{\rho}^{(2)}(t)\rangle\rangle$  evolves to a state with the largest imaginary eigenvalue.

In this 2-site model, the Choi representation of the conditional 2-purity, which can either be conditioned on site 1 or 2, is the boundary state

$$|\mathcal{C}_{2,\mathbf{A}}\rangle\rangle \equiv |\uparrow\uparrow\uparrow\uparrow\rangle\rangle + |\downarrow\downarrow\downarrow\downarrow\rangle\rangle, \quad (31)$$

which is written explicitly on the basis where the first entry is the first replica and Ket-like Choi branch element, the second entry is the first replica bra-like Choi branch one, and the remaining two entries are the duplicate elements in the second replica. Note that this representation is only valid in the restricted Hilbert space of a single particle in the double well.

From Eqs. (31) and (30), one can directly compute the matrix element in Eq. (26). Note that, when diagonalizing  $H_{\text{eff}}$  eigenstates of the eigenvalue with the largest imaginary part, it would yield degenerate eigenvalues. The degeneracy is due to the replica permutation and bra-ket exchange symmetries of  $H_{\text{eff}}$ . Only the eigenstates that are symmetric under the above-mentioned symmetry operation contribute to  $\bar{\mu}_{2,\mathbf{A}}$ . The results are reported in fig. 4.

To discuss the results, consider the post-selected case  $\zeta = 0$ . In this case, We can alternatively solve Eq.(27) by noting that, modulo an overall gauge transformation, we can restrict to the states with real coefficients and parameterise it by  $|\psi(t)\rangle = \cos\theta(t)|\uparrow\rangle + \sin\theta(t)|\downarrow\rangle$ . This

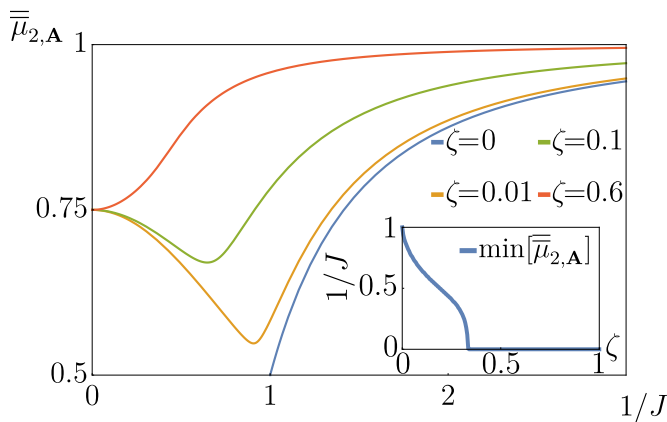


FIG. 4. The steady-state average conditional 2-nd purity,  $\bar{\mu}_{2,\mathbf{A}}$  as a function of the inverse tunnelling strength in a double-well model for various degrees of partial post-selection  $\zeta$ . Lower (higher)  $\bar{\mu}_{2,\mathbf{A}}$  corresponds to more (less) entanglement. For  $\zeta > 0$ ,  $\bar{\mu}_{2,\mathbf{A}}$  is non-monotonous. Inset: location of the minimum of  $\bar{\mu}_{2,\mathbf{A}}$  as a function of  $\zeta$ . The minimum, hence the non-monotonicity, disappears for a weak degree of partial post-selection, i.e. large  $\zeta$ .

parameterization is equivalent to restricting to the  $x-z$  plane of the Bloch sphere, where the North (South) Pole corresponds to  $|\uparrow\rangle$  ( $|\downarrow\rangle$ ). Inserting this expression into Eq.(27), we obtain an equation for the evolution of  $\theta(t)$ :

$$\frac{d\theta}{dt} = J - \sin 2\theta. \quad (32)$$

For  $J < 1$ , the equation admits a steady state  $\theta = \arcsin(J)/2$ , which drifts from the North pole to the equator with increasing  $J$ . Noting that, under the above state parameterization, the half-system purity takes the form  $\mu_{2,\mathbf{A}} = \cos^4 \theta + \sin^4 \theta$ , which can be directly computed from the steady state of Eq. (32). As a result, the entanglement increases (decreasing purity) with increasing  $J$  until it reaches a maximum at  $J = 1$ . We verified that Eq.(27) agrees with the results calculated via  $H_{\text{eff}}$  for  $\bar{\mu}_{2,\mathbf{A}}$ . This is expected as there is one trajectory, and the distortion in Eq.(15) becomes exact.

For  $J > 1$ , Eq. (32) does not admit a steady state solution, and  $|\psi(t)\rangle$  revolves periodically around the Bloch sphere [80]. For any finite  $\zeta$ , however, a stated state distribution of states exists for the stochastic dynamics, with a well-defined trajectory-averaged  $\bar{\mu}_{2,\mathbf{A}}$ . As we include more trajectories with  $\zeta > 0$ , although  $\bar{\mu}_{2,\mathbf{A}}$  no longer represents the true subsystem purity, it still serves as an entanglement measure, and it displays a minimum (i.e. maximum entanglement) at intermediate  $J$ . With increasing  $\zeta$ , the minimum shifts to larger  $J$  (orange and green lines in Fig. 4) and its absolute value increases. The increment in the absolute value can be heuristically understood from the parameterization  $|\psi(t)\rangle = \cos \theta(t) |\uparrow\rangle + \sin \theta(t) |\downarrow\rangle$ , which, when inserted into Eq.(27), induces a  $\theta$  dependence in the Wiener increments with larger weights towards the North Pole.

Hence, the inclusion of more trajectories suppresses entanglement in this 2-site model. It should be noted that this behaviour is not universal but specific to this model.

#### IV. MONITORED GAUSSIAN FERMION MODEL

We now apply the formalism of partial postselection to a specific model where the MiPT has been predicted [18].

In this section, we first present the details of the model (subsection IV A), which consists of a free Majorana fermion chain evolving under random nearest neighbour hopping and subjected to even and odd bond parity continuous measurements. Next, in Sec. IV B, we treat the model within the 2-replica approach following the formalism in Sec. II, and derive the corresponding effective Hamiltonian. Notably, in the limit of strong partial post-selection ( $\zeta \ll \zeta^* = \pi/8$ ), the Hamiltonian can be bosonized. The bosonization procedure is described in Sec. IV C, where we also provide an explicit form of the conditional entropy, which is related to the scaling dimension of the vertex operator. We further derive the renormalization group flow equations for the different gap-opening perturbations. The RG flow allows us to analyze the steady-state long-distance behaviour of the conditional 2nd Renyi entropy in different regimes, which is done in Sec. IV D.

Having derived the field theory that governs the steady state dynamics, we can analyze the MiPTs in the partially-postselected free fermion model, which is done in Sec. V. Specifically, in Sec. V A, we study the features of the measurement-only MiPT driven by the two competing measurements in the absence of unitary evolution. We compare our analytic predictions with numerical simulations in Fig. 7, which shows agreement in the region of applicability of the field theory. In Sec. V B, we examine how the phase diagram is altered in the presence of unitary evolution. The results are summarized in Fig. 9, showing that the extensive-scaling region expands with increasing  $\zeta$ .

##### A. The model

The model, sketched in Fig. 1, consists of a chain of real Majorana fermions with unitary dynamics governed by random (Gaussian white noise) nearest-neighbour hopping and continuous weak measurement of odd and even bond parity. In the Wiener-to-non-Hermitian mapping introduced in Sec. II B (cf. Appendix B), the dynamics of the model are governed by a non-Hermitian random Hamiltonian given by (see also Eq.(B.9) and (29))

$$H(t) = \sum_j^L [J_j(t) + iM_j(t)] i\chi_j \chi_{j+1} \quad (33)$$

and  $L$  (even) is the length of the chain, which is always even.  $J_j(t)$  and  $M_j(t)$  are Gaussian random variables in space and time with

$$\mathbb{E}_G[J_j(t)] = 0, \quad \mathbb{E}_G[J_j(t)J_{j'}(t')] = J^2\delta(t-t')\delta_{j,j'}, \quad (34)$$

and the properties of the non-Hermitian Gaussian noise  $M_j(t)$  follow from Eq.(19) to give

$$\begin{aligned} \mathbb{E}_G[M_j(t)] &= (1-\zeta)\Xi_j, \\ \mathbb{E}_G[M_j(t)M_{j'}(t')] &= \zeta\Xi_j\delta(t-t')\delta_{j,j'} \\ &\quad + (1-\zeta)^2\Xi_j\Xi_{j'}, \end{aligned} \quad (35)$$

where the partial post-selection, controlled by  $1-\zeta$ , determines the mean of the Gaussian measure.

The measurements are grouped into two non-commuting sets: the odd and even bond parity measurements with respective measurement strengths controlled by  $\Xi_j = 1 + (-1)^j\Delta$ , where the dimerization  $-1 \leq \Delta \leq 1$  controls their relative strengths.

This model has been investigated in the monitored limit  $\zeta = 1$  in Ref. 18. It was predicted to undergo MiPTs between area and  $\log^2$ -scaling entanglement entropy as a result of the competition between unitary dynamics and measurement. The model's measurement-only limit,  $J = 0$ , consisting of two sets of competing measurements, coincides with the one investigated in Ref. 10. This measurement-only MiPT shows a peculiar dynamical critical exponent in the full monitored limit, which differs from the projective counterpart (of a percolation universality class [34, 39] [81]) and the fully-post-selected limit (of Ising universality class [10]).

Following the description in Sec. II B, we can rewrite the  $n$ -replicated un-normalised density matrix (of  $n$ -replicated Majorana chains) as a state of  $2n$  replicated Majorana chains. The average dynamics of this state follow Eq.(23), which, as shown in Sec. III, leads to the study of an effective Hamiltonian.

## B. Two-replica and effective spinful fermion model

Following Sec. II, in the rest of the paper, we will analyze the MiPT in the two-replica averaged dynamics. The quantity of interest is now the 2-replica *conditional* purity, Eq.(26).

From Eq.(23) with  $n = 2$ , the evolution of  $|\check{\rho}^{(2)}(t)\rangle\rangle$  becomes

$$\begin{aligned} |\check{\rho}^{(2)}(t)\rangle\rangle &= \mathbb{E}_G[(K(t) \otimes K^*(t))^{\otimes 2}] |\rho^{(2)}(0)\rangle\rangle \\ &= e^{-\mathcal{H}t} |\rho^{(2)}(0)\rangle\rangle. \end{aligned} \quad (36)$$

The effective Hamiltonian  $\mathcal{H}$ , obtained by Gaussian av-

eraging (see Appendix C) is given by

$$\begin{aligned} \mathcal{H} &= \sum_j \frac{J^2}{2} \left( \sum_{\substack{s=\uparrow,\downarrow \\ a=1,2}} \mathcal{P}_{i,i+1}^{(sa)} \right)^2 - \sum_J \frac{\zeta\Xi_j}{2} \left( \sum_{\substack{s=\uparrow,\downarrow \\ a=1,2}} s\mathcal{P}_{i,i+1}^{(sa)} \right)^2 \\ &\quad - \sum_{\substack{s=\uparrow,\downarrow \\ a=1,2}} \sum_j s(1-\zeta)\Xi_j\mathcal{P}_{i,i+1}^{(sa)}, \end{aligned} \quad (37)$$

where  $\mathcal{P}_{i,i+1}^{(sa)} = i\chi_i^{(sa)}\chi_{i+1}^{(sa)}$  is the parity operator of the pair of Majorana fermions  $\chi_j^{(sa)}$  and  $\chi_{j+1}^{(sa)}$  in the replicated space, and  $s = \uparrow (+), \downarrow (-)$  labels the ket and bra space,  $a = 1, 2$  labels the replica index. Note that these newly-introduced Majorana operators differ from the ones in (33) by a Klein factor (an additional ‘Pauli’ string across replica) to ensure proper anti-commutation following the convention in Ref. 18 and 66. The definition of  $\chi_j^{(sa)}$  in terms of the original degrees of freedom is given in Appendix C. With the newly-defined Majorana fermions, the state  $|\mathcal{C}_{2,\mathbf{A}}\rangle\rangle$  in Eq. (26) admits the form [66]

$$|\mathcal{C}_{2,\mathbf{A}}\rangle\rangle \equiv \hat{\mathcal{C}}_{2,\mathbf{A}} |\mathbb{I}\rangle\rangle = e^{\frac{\pi}{4} \sum_{j \in \mathbf{A}} \chi_j^{(1)} \chi_j^{(2)}} |\mathbb{I}\rangle\rangle. \quad (38)$$

Here, the equivalent sign indicates that this expression is only valid when the operator  $\hat{\mathcal{C}}_{2,\mathbf{A}}$  acts on the state  $|\mathbb{I}\rangle\rangle$ , as detailed in Appendix F. Eq.(38) indicates that the computation of  $\overline{\mu}_{2,\mathbf{A}}$  is associated with the parity of  $\downarrow$  fermionic degrees of freedom in  $\mathbf{A}$ ; This relation becomes apparent when expressed in terms of complex fermions; see below.

From Eq.(36), it can readily be seen that the average replica dynamics follow an imaginary time evolution, and thus  $|\check{\rho}^{(2)}(t \rightarrow \infty)\rangle\rangle$  is determined by the low energy physics of  $\mathcal{H}$ , in particular by its ground state and gap properties.

To determine the low energy structure of  $\mathcal{H}$  in Eq.(37), we note that  $\mathcal{H}$  describes an interacting fermionic model with a global  $O(2) \times O(2)$  symmetry. The two  $O(2)$  symmetries are generated by the operators  $\sum_j i\chi_j^{\uparrow 1} \chi_j^{\uparrow 2}$  and  $\sum_j i\chi_j^{\downarrow 1} \chi_j^{\downarrow 2}$ , and they correspond to rotation among  $n$  Majorana operators within the ket ( $s = \uparrow$ ) and bra ( $s = \downarrow$ ) sector. In the absence of PPS,  $\zeta = 1$ , the global symmetry is larger with  $O(2) \times O(2) \times \mathbb{Z}_2$ , and is further enlarged for measurement-only or unitary-only cases [18, 66]. The two  $O(2)$  symmetries indicate two conserved  $U(1)$  charges. These in turn, can be interpreted as the conservation of fermion number of two distinct fermions species given by [66]

$$\begin{aligned} c_{j,\uparrow}^\dagger &= \frac{\chi_j^{(\uparrow 1)} + i\chi_j^{(\uparrow 2)}}{2}, \\ c_{j,\downarrow}^\dagger &= \frac{\chi_j^{(\downarrow 1)} - i\chi_j^{(\downarrow 2)}}{2} \end{aligned} \quad (39)$$

and the two conserved  $U(1)$  charges appear explicitly as  $[\sum_j c_{j,s}^\dagger c_{j,s}, \mathcal{H}] = 0$ , with  $s = \uparrow$  or  $\downarrow$ .

Expressing the Hamiltonian in eq. (37) in terms of these two fermion species, we arrive, after some algebraic manipulation, at the following spinful fermion Hamiltonian (detailed in appendix E)

$$\begin{aligned} \mathcal{H} &= H_{umk} + H_m + H_0 \\ H_{umk} &= \sum_j -4(\zeta \Xi_j + J^2) \sum_{s=\uparrow, \downarrow} (c_{j,s}^\dagger c_{j,s} - \frac{1}{2}) \times \\ &\quad (c_{j+1,s}^\dagger c_{j+1,s} - \frac{1}{2}) \\ H_m &= \sum_j 4(\zeta \Xi_j - J^2) (c_{j,\uparrow}^\dagger c_{j+1,\uparrow} + c_{j+1,\uparrow}^\dagger c_{j,\uparrow}) \times \\ &\quad (c_{j,\downarrow}^\dagger c_{j+1,\downarrow} + c_{j+1,\downarrow}^\dagger c_{j,\downarrow}) \\ H_0 &= - \sum_j 2(1 - \zeta) \Xi_j \sum_{s=\uparrow, \downarrow} (c_{j,s}^\dagger c_{j+1,s} + c_{j+1,s}^\dagger c_{j,s}). \end{aligned} \quad (40)$$

In the language of Eq.(39), the operator  $\hat{\mathcal{C}}_{2,\mathbf{A}}$  in Eq.(38) admits a simple expression as

$$\hat{\mathcal{C}}_{2,\mathbf{A}} |\mathbb{I}\rangle \equiv e^{-i\frac{\pi}{2} \sum_{j \in \mathbf{A}} (c_{j,\uparrow}^\dagger c_{j,\downarrow} - \frac{1}{2})} |\mathbb{I}\rangle. \quad (41)$$

Once again, the equivalent sign indicates that the operator representation is to be understood only when acting on the state  $|\mathbb{I}\rangle$ . Hereafter, we also assume the region  $\mathbf{A}$  to be continuous for simplicity.

To address the ground-state properties and phases of  $\mathcal{H}$ , we note that  $\mathcal{H}$  is number conserving in both spin-up and spin-down fermion species, and the long wavelength (low energy) physics of (40) depends on the particle number, or, more precisely, on the filling factor. The latter is determined by the initial state  $|\mathbb{I}\rangle$ , see (26), which is in the half-filling sector, as shown in Appendix E. We therefore analyse the half-filling ground state of  $\mathcal{H}$ .

In the monitored limit of  $\zeta = 1$ , one takes the freedom to choose  $|\rho(0)\rangle$  within the same representation as  $|\mathbb{I}\rangle$  and  $|\mathcal{C}_{2,\mathbf{A}}\rangle$ , so that  $\rho(0) \propto \mathbb{I}$ , which allows one to obtain an exact solution. With the condition  $\zeta = 1$ , the Hamiltonian has an enlarged symmetry, since the local total parity across all replica,  $\mathcal{R}_j = \prod_{a=1}^2 i\chi_j^{(\uparrow a)} \chi_j^{(\downarrow a)}$  is conserved and the Hamiltonian is invariant under an extra global  $\mathbb{Z}_2$  symmetry in the Choi space:  $\chi_j^{(\uparrow a)} \longleftrightarrow \chi_j^{(\downarrow a)}$  (this generalises to  $n$  replica as well [18]). In this case, the Hamiltonian can be expressed entirely as a function of local  $SO(4)$  generators written in Majorana operators,

$$S_j^{\alpha,\beta} = \frac{i}{2} [\chi_j^\alpha, \chi_j^\beta], \quad (42)$$

and the states  $|\mathbb{I}\rangle$  and  $|\mathcal{C}_{2,\mathbf{A}}\rangle$  isolate the spin representation among different irreducible representations [18]. In Appendix D, we demonstrate an alternative way to obtain the exact solution where a mapping to an integrable model can be constructed via 2 different spin-1/2

operators analogous to the  $\eta, \Sigma$  spin from the Hubbard model [82]. In the monitored case, we show that (37) is equivalent to

$$\begin{aligned} \mathcal{H} \propto \sum_{\substack{\Theta=\Sigma, \eta \\ j=1}}^L \frac{1}{2} (1 + \delta(-1)^j) [\Theta_j^+ \Theta_{j+1}^- + \Theta_j^- \Theta_{j+1}^+] \\ + J_{z,j} \Theta_j^z \Theta_{j+1}^z, \end{aligned} \quad (43)$$

where  $\delta = \frac{\Delta\zeta}{16(J^2 + \zeta)}$ ,  $J_{z,j} = \frac{J^2 - \zeta \Xi_j}{J^2 + \zeta \Xi_j}$ . Eq.(43) corresponds to 2 decoupled  $XXZ$  spin-1/2 chains and its exact solution can be computed via standard means [69].

### C. Strong PPS and bosonisation

An analytical solution of the ground state of Eq. (40) is not available. However, in the strong partial-post-selected limit,  $1 \gg \zeta/(1 - \zeta)$ ,  $J^2/(1 - \zeta)$ , and half-filling condition of interest here, the spectrum of excitation is approximately linear, and the problem can be treated within the standard abelian bosonization procedure [69]. This amounts to linearising the fermion operator around the Fermi surface

$$c_{j,s} \approx e^{-ik_F x_j} \tilde{\psi}_{\mathbf{R},s}(x_j) + e^{ik_F x_j} \tilde{\psi}_{\mathbf{L},s}(x_j), \quad (44)$$

and introducing the bosonic fields  $\theta_s$  and  $\phi_s$  via [83]

$$\begin{aligned} \tilde{\psi}_{\mathbf{L},s}(x) &\approx \frac{1}{\sqrt{2\pi\alpha}} e^{i(\phi_s(x) + \theta_s(x))}, \\ \tilde{\psi}_{\mathbf{R},s}(x) &\approx \frac{1}{\sqrt{2\pi\alpha}} e^{-i(\phi_s(x) - \theta_s(x))}, \end{aligned} \quad (45)$$

where  $\tilde{\psi}_{\mathbf{L}/\mathbf{R},s}(x)$  is the slowly varying part of left/right movers of the fermion, and  $\alpha$  is the UV cutoff of the continuum field theory, of the order of the lattice spacing which has been implicitly taken as  $a = 1$  (the constant of proportionality vanishes in the thermodynamic limit) [69]. The low energy properties of  $\mathcal{H}$  are described by the linearized bosonic Hamiltonian.

The full bosonization procedure for  $\mathcal{H}$  is reported in appendix E which leads to the low energy effective Hamiltonian

$$\begin{aligned} \mathcal{H}_{\text{bos}} \approx \sum_{\epsilon=\sigma,\rho} \left[ \frac{1}{2\pi} \int_x u_\epsilon K_\epsilon (\nabla \theta_\epsilon)^2 + \frac{u_\epsilon}{K_\epsilon} (\nabla \phi_\epsilon)^2 \right] \\ + \sum_{\epsilon=\sigma,\rho} \int_x \frac{2g_\epsilon}{(2\pi\alpha)^2} \cos(\sqrt{8}\phi_\epsilon) \\ + \frac{2g_2}{(2\pi\alpha)^2} \int_x \sin(\sqrt{2}\phi_\rho) \cos(\sqrt{2}\phi_\sigma), \end{aligned} \quad (46)$$

where  $\phi_\rho = \frac{\phi_\uparrow + \phi_\downarrow}{\sqrt{2}}$  and  $\phi_\sigma = \frac{\phi_\uparrow - \phi_\downarrow}{\sqrt{2}}$  are the charge and spin sectors fields. The coupling constants and Luttinger

parameters are given by

$$\begin{aligned}
u_\rho K_\rho &= u_\sigma K_\sigma \equiv v_F = 4(1 - \zeta), \\
\frac{u_\rho}{K_\rho} &= v_F - \frac{32aJ^2}{\pi}, \\
\frac{u_\sigma}{K_\sigma} &= v_F - \frac{32a\zeta}{\pi}, \\
g_\rho &= -g_\sigma = -16(\zeta - J^2), \\
g_2 &= 16a\Delta((1 - \zeta)\pi - \zeta),
\end{aligned} \tag{47}$$

where  $\Delta$  is the dimerization,  $v_F$  is the effective Fermi velocity in the non-interacting case (e.g. from  $H_0$  in Eq. (40)), and  $a$  the lattice constant can be set to unity,  $a = 1$ . In deriving Eq. (46), we keep only the most relevant operator. In particular, we discard highly irrelevant (in the RG sense) terms  $\propto \cos(4\phi_{\uparrow,\downarrow})$  originating from the *umklapp* terms in the Hamiltonian  $H_{umk}$ . We also retain only slow oscillating term with  $0-k_F$  and  $4-k_F$  components around the filling factor  $k_F = \pi/2a$ .

The expected validity of the bosonization treatment in the strong post-selected limit  $1 \gg J^2/(1 - \zeta), \zeta/(1 - \zeta)$  is confirmed by Eq. (47). Indeed the charge and spin Luttinger parameters  $K_\rho, K_\sigma$  diverges at  $J^2/(1 - \zeta) \equiv \mathcal{J}^{*2} = \pi/8$  and  $\zeta/(1 - \zeta) \equiv \zeta^*/(1 - \zeta^*) = \pi/8$  respectively. This also constrains other parameters in Eq.(47) so that the sign of  $g_2$  is the same as  $\Delta$ .

Although the divergence point  $\zeta^*$  is beyond the regime of applicability of perturbation theory  $\zeta \ll 1$ , we expect that the physical picture it implies remains qualitatively correct. Indeed, a similar scenario arises when analysing the *XXZ*- spin 1/2 chain using bosonization[69]. For the *XXZ* chain, while the bosonization analysis fails to capture the value of the phase boundary (calculated using Bethe-ansatz), it does allow to characterize the properties of the different phases [84]. On this ground, the divergence of  $K_\rho$  or  $K_\sigma$  hints at the onset of a phase boundary, though we expect that the location of the phase boundaries to be generically different from  $\zeta^*$  and  $\mathcal{J}^{*2}$ . The indication of a phase boundary from bosonisation is confirmed by numerical finite-size scaling results for measurement-only MiPTs reported in Sec. V.

Within the bosonized theory in (46), the ground-state phases of  $\mathcal{H}_{\text{bos}}$  are obtained by the RG flow of the parameters  $J^2$  and  $\zeta$ , which can be computed within standard methods [69, 85, 86], noting that Eq. (46) is the Hamiltonian of a Sine-Gordon model [69]. Here we follow the procedures in [69, 86] performing real space coarse-graining of the correlator of a pair of vertex operators i.e.  $\langle \exp[-ia\phi(r_1)] \exp[-ia\phi(r_2)] \rangle_{\mathcal{H}}$ . The details of the calculation are reported in Appendix G. In the analysis below, we will separate the no-dimerization case  $\Delta = 0$ , from the general case. In the former,  $g_2 = 0$  identically (cf. Eq.(47)), so that it cannot be simply obtained as a limit of the general case for  $\Delta \rightarrow 0$ . For no-dimerization,  $\Delta = 0$ ,  $g_\rho$  and  $g_\sigma$  flows separately, and the perturbative

RG flow up to second order in  $g_\epsilon$  and  $K_\epsilon$  gives

$$\begin{aligned}
\partial_l K_\epsilon &= -\frac{y_\epsilon^2 K_\epsilon^2}{2} \\
\partial_l y_\epsilon &= (2 - 2K_\epsilon)y_\epsilon, \\
y_\epsilon &= \frac{g_\epsilon}{\pi u_\epsilon}, \quad \epsilon = \sigma, \rho
\end{aligned} \tag{48}$$

where  $l$  is the logarithm of the RG time. In the most crude analysis in first order of  $g_\epsilon$ , the coupling for  $\cos \sqrt{8}\phi_\epsilon$  is irrelevant for the physically relevant scenario  $K_\epsilon > 1$ . However, accounting for the flow for  $K_\epsilon$  can result in one of the modes being gapped but not both simultaneously, as we numerically evaluate the RG flows.

For  $\Delta > 0$ , the  $g_2$  term is more relevant than the  $g_\epsilon$  since the cosine of the former is with higher frequency, so we can safely discard the  $\cos(\sqrt{8}\phi)$  terms in H. The RG flow equations, in this case, are derived in Appendix G following a standard procedure, which leads to

$$\begin{aligned}
\partial_l K_\rho &= -\frac{g_\rho^2 K_\rho^2}{16\pi^2 u_\rho^2} \frac{I(\mu_\rho, K_\sigma, \sqrt{2})}{2\pi}, \\
\partial_l K_\sigma &= -\frac{g_\sigma^2 K_\sigma^2}{16\pi^2 u_\sigma^2} \frac{I(\mu_\sigma, K_\rho, \sqrt{2})}{2\pi}, \\
\partial_l g_2 &= \left( 2 - \frac{1}{2}(K_\rho + K_\sigma) \right) g_2,
\end{aligned} \tag{49}$$

where

$$\begin{aligned}
\left( \frac{u_\sigma}{u_\rho} \right)^2 &= 1 + \mu_\rho, \\
\left( \frac{u_\rho}{u_\sigma} \right)^2 &= 1 + \mu_\sigma \\
I(\mu, K, \beta) &= \int_{-\pi}^{\pi} d\theta \left( \frac{1}{1 + \mu \cos \theta} \right)^{\frac{\beta^2 K}{4}}.
\end{aligned} \tag{50}$$

The RG flow in Eqs. (50,48) dictate the low energy physics of the model and are used in the next section to characterize the properties of the MiPT in the partial-post-selected model.

#### D. Conditional 2nd Rényi entropy

We are now able to determine the ground-state properties of the effective Hamiltonian in Eq.(46) from the RG flows, Eq.(49) and (48). As the ground state properties determine the entanglement scaling, we expect the entanglement to scale logarithmically in the critical phase and as an area law in the gapped phase. Below we confirm these expectations by calculating  $S_{2,\mathbf{A}}^{(cond)}$ . The calculation involves the action of  $\hat{\mathcal{C}}_{2,\mathbf{A}}$  on the state  $|\mathbb{I}\rangle$  (cf Eq.(38) and (41)), which can be mapped to a 2-point vertex correlation.

Under bosonisation, the operator  $\hat{\mathcal{C}}_{2,\mathbf{A}}$  becomes a pair of vertex operators (excluding fast oscillating terms):

$$\hat{\mathcal{C}}_{2,\mathbf{A}} \equiv e^{i\frac{1}{2}(\phi_\downarrow(x_r) - \phi_\downarrow(x_l))}, \tag{51}$$

and the exponential of the conditional 2nd Renyi entropy (cf Eq.(15)) appears as

$$\begin{aligned}
& e^{-S_{2,\mathbf{A}}^{(cond)}} \\
&= \langle\langle \mathcal{C}_{2,\mathbf{A}} | \rho^{(2)}(t \rightarrow \infty) \rangle\rangle \\
&= \lim_{t \rightarrow \infty} \langle\langle \mathbb{I} | e^{i\frac{1}{2}(\phi_{\downarrow}(x_r) - \phi_{\downarrow}(x_l))} e^{-t\mathcal{H}} | \mathbb{I} \rangle\rangle \\
&\sim \langle\langle \text{GS} | e^{i\frac{1}{2}(\phi_{\downarrow}(x_r) - \phi_{\downarrow}(x_l))} | \text{GS} \rangle\rangle \\
&= \langle\langle \text{GS} | e^{i\frac{1}{2\sqrt{2}}[\phi_{\rho}(x_r) - \phi_{\rho}(x_l)]} e^{-i\frac{1}{2\sqrt{2}}[\phi_{\sigma}(x_r) - \phi_{\sigma}(x_l)]} | \text{GS} \rangle\rangle. \tag{52}
\end{aligned}$$

In the fourth line, we replace the boundary state  $\langle\langle \mathbb{I} |$  by the ground state of  $\mathcal{H}$ , which is equivalent up to a length independent constant, see Appendix F.

From Eq.(52), we can readily extract the scaling of  $S_{2,\mathbf{A}}^{(cond)}$ . If both sectors are gapless, we have that [69]

$$e^{-S_{2,\mathbf{A}}^{(cond)}} = \left( \frac{\alpha}{x_r - x_l} \right)^{\frac{K_{\sigma} + K_{\rho}}{16}}, \tag{53}$$

where  $\alpha$  is the UV cutoff. This demonstrates the logarithmic scaling of  $S_{2,\mathbf{A}}^{(cond)}$ . If both sectors are gapped (cosine potential is relevant), the field  $\phi_{\sigma}$  and  $\phi_{\rho}$  are locked in one of the minima of the potential. Hence, the configuration of  $\phi$  fields is fixed, and the vertex correlation becomes a constant, giving an area law for  $S_{2,\mathbf{A}}^{(cond)}$ .

If only one of the sectors is gapped and the Hamiltonian remains separable,  $S_{2,\mathbf{A}}^{(cond)}$  remains logarithmically scaling. In contrast, the gapped sector gives a constant in the vertex correlation (52), the gapless sector contributes a power law decay leading to logarithmic scaling of  $S_{2,\mathbf{A}}^{(cond)}$ .

## V. MEASUREMENT-INDUCED PHASES AND THEIR TRANSITIONS

We are now in the position to use the Hamiltonians (43,46), along with the RG-flow equations (48, 49) to characterize the steady-state phases of partially post-selected dynamics of the Gaussian model in Eq.(33). We study both the measurement-only dynamics ( $J = 0$ ) and unitary-measurement-induced phases ( $J^2 > 0$ ), and we discuss them separately hereafter.

### A. Measurement-only dynamics

In the absence of unitary dynamics,  $J = 0$ , the system is evolving entirely according to two competing sets of measurements: the set of odd and the set of even bond measurements. Notably, the  $J = 0$  limit of the model (33) coincides with the measurement-only case studied in Refs. 10 and 18 where monitored and post-selected limits follow very different behaviours. In particular, finite-size

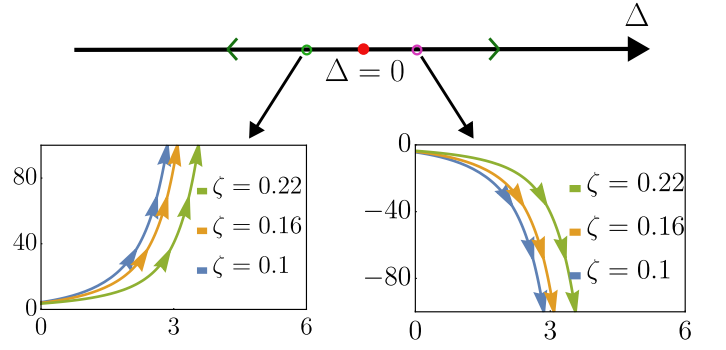


FIG. 5. Schematic phase diagram for the measurement-only dynamics determined by the dimerization  $\Delta$ . The arrows indicate the RG flow to the two distinct fixed points  $\Delta = \pm 1$  with a critical point (red dot) at  $\Delta = 0$ . The plots show The RG flow of  $g_2$  from (49) evaluated at different points (green and purple circles), indicating that the interaction is relevant in both cases, and it leads to area law of phases.

scaling reveals that the monitored system belongs to a different universality class from the fully post-selected model [10].

*a. Post-selected limit*— The fully post-selected dynamics are obtained by setting  $\zeta = 0$  in Eq.(37), and the physics is entirely dictated by  $\Delta$ . The effective Hamiltonian now reads:

$$\mathcal{H} = - \sum_{\substack{s=\uparrow,\downarrow \\ a=1,2}} \sum_j s(1 + \Delta(-1)^j) i\chi_j^{(sa)} \chi_{j+1}^{(sa)}, \tag{54}$$

Using the usual Jordan-Wigner transformation, the imaginary time evolution is, therefore, equivalent to 2 decoupled 1D traverse field Ising models in either the bra ( $s = \downarrow$ ) or ket ( $s = \uparrow$ ) space.

The critical properties of the post-selected dynamics fall in the Ising universality class, and the critical exponent  $\nu$  that determines the divergence of the correlation length  $\xi \sim |\Delta|^{-\nu}$ , is  $\nu = 1$ . Away from criticality for  $\Delta > 0$ , the even parities are measured more strongly, and this phase is characterised by a pair of entangled Majorana fermions residing at the edges of a finite-length chain. This phase is associated with a  $\log_2$  topological entanglement entropy per replicated chain in the area-law phase.

On the other side  $\Delta < 0$ , the odd parities measurements are stronger, and it features all Majorana being measured in pairs. This, therefore, corresponds to a topologically trivial phase with vanishing topological entanglement entropy.

*b. Strong post-selection* — When  $\zeta \neq 0$ , the system no longer follows the deterministic dynamics from Eq.(54), but stochastic fluctuations inherent to the measurement process enter the system dynamics. With the partial post-selection introduced in Eq. (9), the parameter  $\zeta$  controls the amount of fluctuations (i.e. the fraction of quantum trajectories) allowed in the system's dynamics. We can analyse the strong post-selected limit  $\zeta \ll 1$

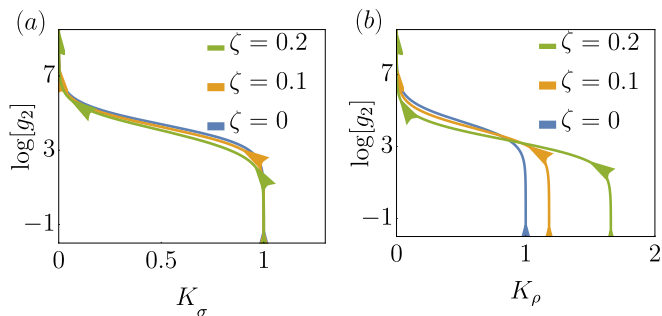


FIG. 6. RG flow of the dimerised measurement-only dynamics (49) in the  $g_2 - K_\sigma$  plane (a) and  $g_2 - K_\rho$  plane (b) for  $\Delta = 0.01 > 0$  and different degree of partial post-selection,  $\zeta$ . Finite partial-post-selection flows (green and orange curves) channel into the no-post-selection one (blue curve). For  $\Delta < 0$ , the flow is reflected along the  $g_2 = 0$  axis.

with the bosonized Hamiltonian (46). As argued in Sec. IV C, the steady state of the system is governed by different equations for  $\Delta = 0$  and  $\Delta \neq 0$ , so we address them separately.

For  $|\Delta| > 0$ , using the flow in (49), we observe that the cosine term parametrized by the  $g_2$  coupling is in general relevant for  $K_\rho + K_\sigma < 4$ , which we confirm by evaluating Eq.(49) numerically. The results are shown in Fig. 5 for different values of  $\zeta$ , plotted against the logarithm of the RG time  $l$ . The unbounded growth in the coupling  $g_2$ , which does not change sign along the RG flow, indicates a massive/gapped phase.

The RG flows in the  $K_\rho - g_2$  plane and  $K_\sigma - g_2$  plane for  $\Delta \neq 0$  are depicted in Fig. 6. These shows that the flow of PPS dynamics  $\zeta > 0$  merges with the flow of post-selected limit  $\zeta = 0$ , resulting in massive (gapped) phases. The merging of the RG flow of the two models indicates that the steady-state physics of the strong PPS model  $\zeta > 0$  coincides with that of the fully post-selected one  $\zeta = 0$ .

In addition, the flow gives an energy gap scaling, which is entirely determined by the long RG time Luttinger parameters  $K_\sigma$  and  $K_\rho$  [69]. The fact that the two models follow the same gap scaling in the long time limit, therefore predicts the same (Ising) universality of the MiPT in the post-selected and strong PPS dynamics.

This means that that the strong-PPS gapped phase at finite  $\zeta$  with  $\Delta > 0$  ( $\Delta < 0$ ) is continuously connected to the gapped phase  $\zeta = 0, \Delta > 0$  ( $\zeta = 0, \Delta < 0$ ) of the post-selected model. The points  $|\Delta| = 1$  are the two only stable fixed points in the measurement-only dynamics, as reported in the phase diagram in Fig. 5. We, therefore, expect that the universal properties of the strong-partial post-selected regime are inherited from Eq. (54), i.e. those of two uncorrelated copies of an Ising model.

This is the first main prediction of our theory: The MiPT remains in the same Ising-like universality class for finite  $\zeta$  as long as the bosonized approximation for the theory remains valid. Physically, this predicts the stability of the post-selected MiPT universal fea-

ture against (weak) fluctuations induced by the measurement's stochasticity.

For  $\Delta = 0$ ,  $J = 0$ , Eq.(49), together with the definition of Luttinger parameters in Eq.(47), implies that the  $g_2 = 0$ , and that the  $\sigma$ - and  $\rho$ -modes decouple. The RG-flow is then standard [69], with the  $\rho$ -mode flowing to a massive phase ( $g_\rho \rightarrow \infty$ ), while the  $\sigma$ -mode, following an expansion around  $K_\sigma \rightarrow 1^+$ , flows to  $g_\sigma \rightarrow 0$ ,  $K_\sigma > 1$ . Correlations in the overall theory are thus dominated by the  $\sigma$ -mode, which is a Gaussian-free theory displaying free Luttinger liquid criticality. The scaling of  $S_{2,A}^{(cond)}$  follows from Eq.(53), which implies a logarithmic scaling with a pre-factor proportional to  $K_\sigma$ . We note that a logarithmic scaling is observed numerically in entanglement entropy, indicating that the robustness of Ising universality, as predicted by the analytics, applies to other entanglement measures.

*c. From strong post-selection to monitored dynamics*— In the post-selected limit, ( $\zeta = 0$ ) the transition for the system's entanglement entropy follows an Ising universality similar to the conditional entropy. Our bosonized theory for the latter predicts that the Ising-like transition persists when moving away from the post-selected limit. Meanwhile, studies of the system entanglement entropy for the fully monitored case ( $\zeta = 1$ ) show a measurement-only transition of a different nature [18] with a critical exponent of  $\nu = 5/3$  [10]. Although our bosonised theory cannot access the full transition between the post-selected ( $\zeta = 0$ ) and the monitored ( $\zeta = 1$ ) dynamics due to the divergence of the Luttinger parameter at  $\zeta^*$ (cf. Sec. IV C), this divergence indicates a phase boundary separating the Ising-universality from a different universality [69] (as discussed in Sec. IV C).

To further characterize the transition between the post-selected and fully monitored universality in other entanglement measures, we analyze the critical exponent  $\nu : \xi \sim |\Delta|^{-\nu}$  of this measurement-only MiPT via numerical simulation of the free fermion model for generic  $\zeta$ . To efficiently extract the critical exponent numerically, we employ techniques from free fermion simulation [10, 13] and perform finite size scaling analysis of the topological entanglement entropy  $S_{TEE}$  [10, 39, 87–89], as detailed in Appendix H. The results are presented in Fig. 7 showing that  $\nu \approx 1$  for strong PPS before deviating abruptly in a narrow range around  $\zeta \approx \zeta^*$  and approaching  $\nu = 5/3$  when  $\zeta \approx 1$ . Surprisingly, numerical data shows that close to the transition,  $\nu \approx 2.3 > 5/3$ , before dropping back to  $\nu = 5/3$  for larger  $\zeta$ . The results suggest a consistent phase separation scenario for the entanglement entropy MiPTs. Indeed, the stability of the Ising value of the critical exponent  $\nu = 1$  is similar to the region of validity of the bosonised theory, suggesting a common mechanism underpins both phenomena.

*d. Monitored limit,  $\zeta = 1$*  — The monitored limit ( $\zeta = 1$ ) is given by Eq. (43), which, for the measurement only-case  $J = 0$ , reduces to a  $XXZ$ -Hamiltonian with a dimerization in hopping term, also known as spin-Peierls

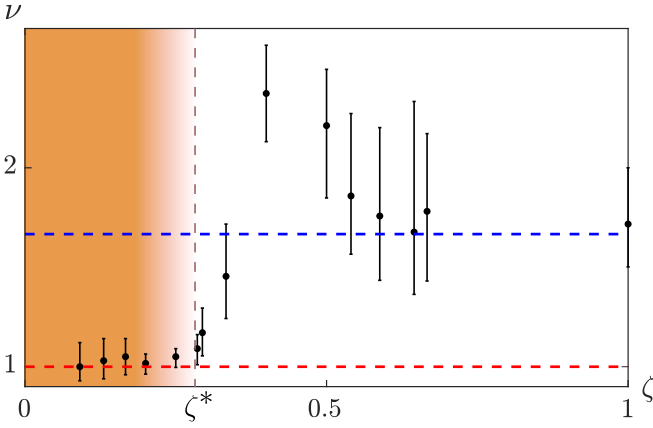


FIG. 7. The critical exponent  $\nu$  of the measurement only phase transition as a function of the degrees of PPS,  $\zeta$ . The pink area marks the regime of validity of the bosonized theory. The dashed horizontal lines mark the known critical exponent for the post-selected model  $\nu = 1$  (red) and monitored dynamics  $\nu = 5/3$  (blue). The fully post-selected Ising critical exponent  $\nu = 1$  is unchanged for a finite range of  $\zeta$  above  $\zeta = 0$ . The abrupt deviation from  $\nu = 1$  occurs in the proximity of the breakdown of the bosonized theory at  $\zeta \approx \zeta^* = 0.28$  (end of the shaded region). The fully monitored critical exponent  $\nu = 5/3$  is recovered for  $\zeta \rightarrow 1$ . The large error bars for increasing  $\zeta$  are due to the large fluctuation due to the increasing trajectory-to-trajectory fluctuations in this regime.

model [69]. This model predicts a BKT transition at  $\Delta = 0$  [69]. This differs from the Ising bosonized theory for the strong PPS. This difference is also consistent with the model's symmetry change in the two limits, as discussed in Sec IV B.

Note that the BKT transition (hence the scaling of the conditional partial purity or entanglement entropy) predicted by Eq. (43) does not capture the correct universality class of the fully monitored dynamics. Indeed, in the limit  $\zeta = 1$ , it has been shown that the 2-replica model differs from the  $n \rightarrow 1$  limit for which the phase transition in the measurement-only limit is not known [18]. However, since for strong PPS, the replicas completely decouple, the post-selected limit is independent of the replica number. We expect that the stability of the post-selected phase and its breakdown should be captured in the 2-replica case considered here.

## B. Partial post-selected monitoring with unitary dynamics

*a. No-dimerization case,  $\Delta = 0$* — To analyze the effect of unitary dynamics on the system, we start by considering the case where dimerization is absent,  $\Delta = 0$ ,  $J^2 > 0$ ,  $\zeta > 0$ . In this case, the RG flow in Eq. (49) keeps  $g_2 = 0$ , the  $\rho$ -mode and  $\sigma$ -mode decouple as indicated by  $H_{bos}$  and Eq. (48), and the Luttinger parameters  $K_\rho$  and  $K_\sigma$  in (47) are both initially larger than unity. At the leading order, the RG flow signals that

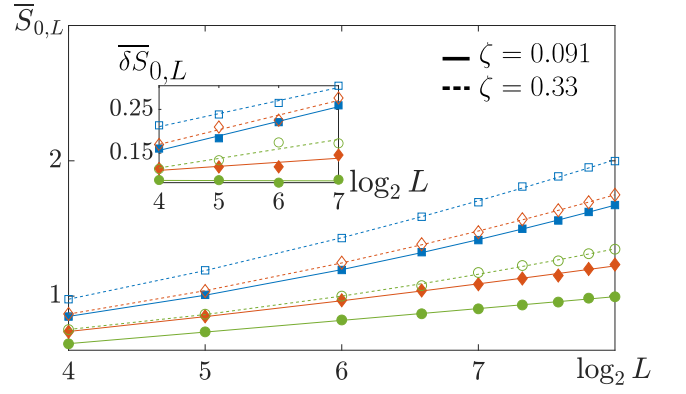


FIG. 8. Trajectory averaged entanglement entropy from numerical simulation at zero dimerization  $\Delta = 0$ . The plot shows the scaling of average half-cut entanglement entropy  $\bar{S}_{0,L}$  as a function of  $\log_2 L$  (where  $L$  is the system size) for two degrees of partial post-selection,  $\zeta = 0.091$  (full markers/solid lines) and  $\zeta = 0.33$  (hollow markers/dashed lines). Different colours correspond to different values of  $J^2$  (divided by an implicit factor  $\gamma + \gamma b = 1$ ), which are 0.091 (green), 0.27 (orange) and 0.45 (blue) for full markers/solid lines, and 0.067 (green), 0.2 (orange) and 0.33 (blue) for hollow markers/dashed lines. Lines are best fit with a second-order polynomial. Inset: average half-cut entanglement entropy difference  $\bar{\delta S}_{0,L} \equiv \bar{S}_{0,2L} - \bar{S}_{0,L}$  for different values of  $J^2$  and  $\zeta$  as in the main plot. Here  $\bar{S}_{0,L}$  follows a  $\log_2 L$  dependence for small  $J^2$  and  $\zeta$  (green full circles), changing into a  $(\log_2 L)^2$  dependence upon increasing  $J^2$  (orange/blue markers) or upon increasing  $\zeta$  (hollow markers). Error bars are within the marker sizes.

$\mathcal{H}_{bos}$  is gapless for  $K_\epsilon > 1$ . Evaluating (48) numerically reveals that one of the sectors is always massless. Given the decoupling between the two sectors,  $\lim_{t \rightarrow \infty} |\check{\rho}^{(2)}(t)\rangle\rangle$  will evolve to a tensor product of two ground states  $|\text{GS}_{\mathcal{H}_\rho}\rangle \otimes |\text{GS}_{\mathcal{H}_\sigma}\rangle$ . Thus, correlations w.r.t.  $\mathcal{H}_{bos}$  are dominated by the gapless sector ground state, which displays power-law decaying length-dependent, signalling a critical scaling of entanglement. More precisely, Eq. (52) directly signals a power decaying dependence for the exponential of  $S_{2,\mathbf{A}}^{(cond)}$ , contributed by the gapless sector vertex-pair correlator. This translates to a logarithmically scaling  $S_{2,\mathbf{A}}^{(cond)}$ . Therefore, we expect that the true entanglement entropy will be dominated by the critical sector and will show a critical entanglement scaling.

This result differs from the predicted  $(\log L)^2$  in Ref. 18 for the fully monitored case. The absence of  $(\log L)^2$  scaling in strong PPS where bosonisation remains valid could be traced back to the breaking of local parity  $\mathcal{R}_j = \prod_a i\chi_j^{(+a)} \chi_j^{(-a)}$ ,  $[\mathcal{R}_j, \mathcal{H}] \neq 0$ , which prohibits one to express  $\mathcal{H}$  solely as local  $\text{SO}(2N)$  generators. Consequently,  $\mathcal{H}$  is no longer described by the non-linear sigma model in [18] that gives the  $(\log L)^2$  scaling.

To confirm a change from  $\log L$  to  $(\log L)^2$  with increasing  $J^2$  and increasing  $\zeta$ , we numerically analyze the scaling of the entanglement entropy along the no-dimerization line. The results are shown in Fig. 8, and

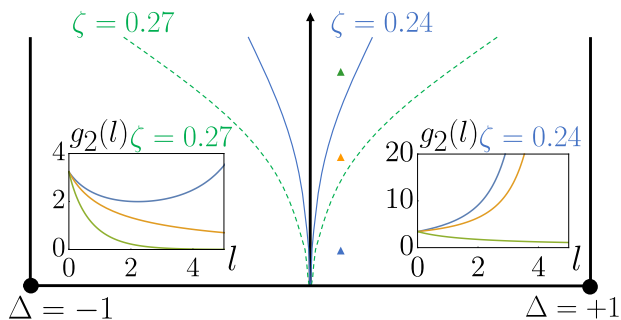


FIG. 9. Schematic phase diagram obtained from the 2-replica approximation RG flow (49). A critical unitary strength  $J_c$  separating the gapped area-law scaling phase ( $J^2 < J_c^2$ ) from the critical logarithmic phase ( $J^2 > J_c^2$ ) as reported for  $\zeta = 0.24$  (green dotted line) and  $\zeta = 0.27$  (blue line). The left and right insets show the flow of  $g_2$  under RG (49) for  $\zeta = 0.24$  and  $\zeta = 0.27$  respectively evaluated at  $J^2 = 0.019$  (blue),  $J^2 = 0.20$  (orange), and  $J^2 = 0.38$  (green), with  $\Delta = 0.1$  in all cases. The irrelevance of  $g_2$  indicates a critical logarithmic scaling entanglement.

here we denote  $S_{0,L}$  as the half-cut entanglement entropy of a system size  $L$ . For weak unitary  $J^2 = 0.091$  and strong PPS  $\zeta = 0.091$  marked in full green circle, the trajectory averaged half-cut entanglement entropy  $\bar{S}_{0,L}$  follows a  $\log_2 L$  dependence. This changes into a  $(\log_2 L)^2$  dependence upon increasing  $J^2$  (orange full diamond/blue full square) or upon increasing  $\zeta$  (dashed line, hollow green circle). For  $\zeta = 0.33$  (dashed lines), which is beyond the validity of our bosonized theory, all lines display a quadratic dependence. To further distinguish the  $\log L$ -scaling from the  $(\log L)^2$  one, we use as an indicator the difference in half-cut entanglement entropy  $\delta S_{0,L} \equiv S_{0,2L} - S_{0,L}$  [18] — cf. Fig. 8 Inset. The two cases are then distinguished by a  $\delta \bar{S}_{0,L} \sim \log L$  vs  $\delta \bar{S}_{0,L} \sim \text{const.}$  dependence respectively (see Appendix H). This analysis demonstrates that increasing the degree of either unitary ( $J^2$ ) or non-unitary ( $\zeta$ ) stochasticity leads to a qualitative change from a log-scaling to a  $(\log)^2$ -scaling of the half-cut entanglement entropy.

The change in the scaling behaviour happens approximately at the point where bosonization is expected to break down  $\zeta^*$  and  $J^{*2}$ . This is consistent with the picture in the previous section, where the breakdown of bosonization at  $\zeta^*$  signals a transition away from the universality of the post-selected model towards the universality of the monitored model, which is captured by the non-linear sigma in Ref. 18.

*b. General monitored-unitary dynamics,  $\Delta \neq 0$*  — For generic strong PPS case with all  $|\Delta| > 0$ ,  $J^2 > 0$ , and  $\zeta > 0$ ,  $g_2$  is the main parameter which controls the entanglement scaling. From a numerical solution of the RG flow Eq.(48), we see that for small initial values,  $g_2$  either flows to irrelevant at large  $J^2$  or grows indefinitely for sufficiently small values of  $J^2$ , (cf. Fig. 9). In the latter case, since the  $g_2$  term is always more relevant than the  $g_\rho$  and  $g_\phi$  terms, the physics is entirely governed by

the  $g_2$  term which opens a gap in the system leading to an area-law phase (cf Eq.(52)). When  $g_2$  flows to zero at large  $J^2$ , the  $g_\epsilon$  coupling term of  $\cos(\sqrt{8}\phi)$  gaps at most one of the two sectors leaving at least one sector being gapless. This phase remains critical, as in the case of  $\Delta = 0$ , and it is continuously connected to the  $\Delta = 0$  line. This suggests that there is a finite region of critical scaling separating the  $\log^2 L$  phase from the area-law, which is different to the monitored limit where the two phases are separated by a singular critical line [18] (see fig. 1 for a schematic sketch). We note that this phase transition from the area-law phase to the finite critical phase would be of BKT-universality [90].

The overall result for the phase diagram from the 2-replica approximation is schematically shown in Fig. 9. For a fixed partial post-selection  $\zeta \neq 1$ , and non-zero dimerization  $\Delta \neq 0$ , we find critical values of  $J^2$  beyond which  $|g_2|$  is irrelevant, corresponding to a critical-scaling phase. This phase expands when retaining a larger subset of quantum trajectories (i.e. increasing  $\zeta$ ). The results from the RG analysis of the 2-replica model are also confirmed by the numerical evaluation of the entanglement entropy scaling in appendix H, Fig. 15. This expansion is understood as a result of the system exploring a larger extent of the Hilbert space as more trajectories are retained. This imposes fewer constraints on the unitary dynamics in generating large-scale entanglement and is consistent with similar numerical findings with deterministic unitary dynamics [10].

## VI. DISCUSSION AND CONCLUSION

In this work, we have analysed the steady-state out-of-equilibrium phases of a monitored many-body quantum system when only part of the measurement readouts is retained (partial post-selection). We have first developed a general equation for the evolution of a quantum system under partial postselection of continuous Gaussian measurements, named Partial-Post-Selected Stochastic Schrödinger Equation (PPS-SSE) — cf. eq.(9), in which a parameter continuously bridges between the fully monitored and fully post-selected limits. Since the two limits are known to give rise to MiPT of different universality classes, we have studied such crossover for a specific model of free Gaussian real fermions with random unitary dynamics. We analyzed the MiPT in a 2-replica approximation which captures the simplest non-linearity in the system's state. Within the approximation, we derive the MiPT in terms of the low energy long-wavelength properties of and associated bosonised Hamiltonian in a 2-replica-Choi-duplicated space in the limit of strong partial post-selection — cf. Eq.(46).

In the strong PPS limit, we predict that the model presents MiPTs from area laws (with distinct quantum order) to a critical phase. We show that for strong yet finite partial post-selection, the phase diagram displays the same universal features as the post-selected model.

In particular, Without unitary dynamics, the transition reduces to an Ising-like transition with a logarithmic critical scaling at the transition point. The entangling phase displays a log scaling instead of  $\log^2$  in Ref. 18, with the only quantitative changes given by the expansion of the phase with critical scaling upon increasing the range of measurement outcomes retained — cf. Fig. 9. Notably, our theory predictions are limited by the validity of the bosonization, which breaks down at finite values of the partial post-selection, indicating a possible phase transition at that point. Numerical results corroborate this finding by showing an abrupt change in the universal scaling of the measurement-only transition at a similar value of partial post-selection — cf. Fig. 7.

Our theory and its prediction shed new light on MiPT. First, the developed PPS-SSE is the first continuous stochastic equation that offers a novel analytical approach to study the relation between the critical phenomena observed in stochastic monitored dynamics and deterministic non-Hermitian evolution, as well as a means to analyze the transition between the two. It can be, therefore, employed to explore the role of multiple trajectories in a variety of MiPTs. The underlying microscopic derivation can also be the basis for obtaining similar PPS for other measurement-induced dynamics, like quantum jumps [53, 55, 58, 91].

Our findings for the Gaussian model indicate that the physics of post-selected measurement dynamics is robust against weak fluctuations induced by measurements. Our results suggest that different trajectories contribute different universal properties to the overall ensemble. It is interesting to explore the generality of this finding and the mechanism underpinning the transition from post-selected to monitored dynamics identified in this work.

Finally, the feasibility of observing robust MiPTs by retaining a fraction of quantum trajectories provides a possible route to tackle the experimental post-selection problem, by performing tomography of the average state of a fraction of trajectories as opposed to tracking the trajectory-by-trajectory entanglement entropy.

## ACKNOWLEDGMENTS

We are grateful to M. Buchhold, S. Diehl, R. Fazio, M. Fava, G. Kells, A. Mesaros, M. Schiro, and X. Turkeshi for their helpful discussions. A.R. acknowledges support from UKRI via Research England Connecting Capability Funded Northwest CyberCom project and from the Royal Society, grant no. IECR2212041. D.M. thanks the GMT group at SPEC CEA, LPTMS CNRS, and Collège de France for their hospitality.

## DATA AVAILABILITY

The data that support the findings of this article are openly available [99].

*Note added.* During the completion of this manuscript, we became aware of a related work by Y. Le Gal, X. Turkeshi, and M. Schirò appearing on arxiv, numerically analyzing the stability of non-Hermitian dynamics in the context of quantum jump equation [92].

## Appendix A: PPS, shifted Gaussian and their time continuum limit

Here, we demonstrate how the time continuum is taken, giving  $\delta\lambda = [(1 - \zeta)/\zeta]\lambda$ . For convenience, we name  $(1 - \zeta)/\zeta = b$  in this appendix:  $\delta\lambda = b\lambda$ . From Eq.(6), the shift in mean  $\delta\lambda$  of  $P_{r_c}$  has the following  $r_c$  dependence

$$\delta\lambda = \Delta \sqrt{\frac{2}{\pi}} \frac{e^{-\frac{(-r_c + \lambda \langle \hat{O}_i \rangle)^2}{2\Delta^2}}}{1 + \text{Erf} \left[ \frac{-r_c + \lambda \langle \hat{O}_i \rangle}{\sqrt{2}\Delta} \right]} \quad (\text{A.1})$$

Since  $\lambda$  scales as  $\lambda \sim \sqrt{dt}$ , we ask what  $dt$ -dependence we need to assign to  $r_c$  so that  $\delta\lambda \sim \sqrt{dt}$ , which matches the scaling of  $\lambda$  in the Kraus operator. In other words, we are solving

$$\frac{e^{-(-x + a \langle \hat{O}_j \rangle \sqrt{dt})^2}}{1 + \text{Erf} \left[ -x + a \langle \hat{O}_j \rangle \sqrt{dt} \right]} = ba\sqrt{dt} \quad (\text{A.2})$$

where  $x = \frac{r_c(dt)}{\sqrt{2}\Delta}$ ,  $a = \frac{\sqrt{\gamma}}{\sqrt{2}\Delta}$ . This choice of parameterising  $\delta\lambda$  ensures that  $r_c$  depends negligibly on  $\langle \hat{O}_j \rangle$  as  $dt \rightarrow 0$  which is advantageous from an experimental point of view. The dependence of  $r_c$  on  $dt$  according to (A.2) is shown in Fig. 10(a), and it can be seen that  $r_c \xrightarrow{dt \rightarrow 0} -\infty$ . Analogous to  $\lambda \xrightarrow{dt \rightarrow 0} 0$  and  $\gamma$  is the parameter that captures measurement backaction, what captures PPS in time continuum is  $b$  from (A.2) and its dependence on  $r_c$  for fixed  $dt$  is shown in Fig. 10(b), and it is lower bounded  $b(r_c = -\infty) = 0$ . Solving for Eq.(A.2), we arrive at Eq.(7).

Under this scaling, we find that the correction to variance also scales like  $\delta \sim \sqrt{dt}$ . However unlike the unmodified mean  $\lambda$  which scales like  $\lambda = \sqrt{\gamma dt}$ , under this parametrization  $\Delta = \mathcal{O}(dt^0)$  and hence we can safely set  $\delta \rightarrow 0$ .

In addition to the two-sample Kolmogorov-Smirnov test on the probability distribution in the main text, we have also verified numerically the shifted Gaussian approximation by considering a 2-qubit toy model. The toy model is described by the Hamiltonian  $H = \sigma_1^+ \sigma_2^- + \sigma_2^+ \sigma_1^-$ , and the 2 qubits are subject to measurement operators  $(\mathbb{I} + (-1)^j \sigma_j^z)/2$ ,  $j = 1, 2$ . Firstly, for fixed  $b$  in Eq.(7), the distributions of the steady state entanglement entropy are computed via two different ways: 1. the update of the state by the measurement operators is given by Eq.(2) with the probability distribution  $P_{r_c}(x_j)$  given by the truncated Gaussian, 2. the update of the state is

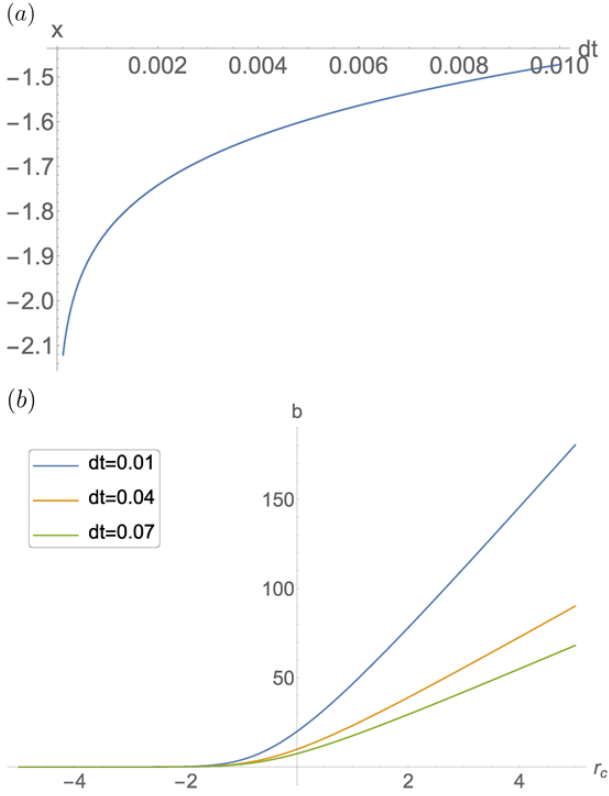


FIG. 10. (a): dependence of  $x$ , from (A.2), on  $dt$ , with  $b = 1$  and  $\langle \hat{O}_j \rangle = 0.1$ . It can be seen that  $r_c \sim x$  approaches  $-\infty$  in the time continuum limit  $dt \rightarrow 0$ . (b): dependence of  $b$ , from (A.2), on  $r_c$  for various  $dt$ . As  $dt$  decreases, the same  $b$  corresponds to a  $r_c$  in the more negative direction.

computed via Eq.(9). Then, the 2 distributions are compared using the Two-sample Kolmogorov-Smirnov test. This is repeated for different values of  $\Delta t$ , the time increment used. The results are shown in Fig. 11.

For completeness, we also display numerically the samplings from the truncated and shifted Gaussian in Fig. 12, together with the associated p-values calculated. It displays statistical equivalence for  $dt = 0.001$ .

## Appendix B: Continuous measurement as non-Herm noises and PPS on Gaussian average

The procedures we are using here is an extension to [18], and we make explicit link to the discrete time description of continuous measurement in (2), and extending it to PPS. To begin with, we start from (2) and

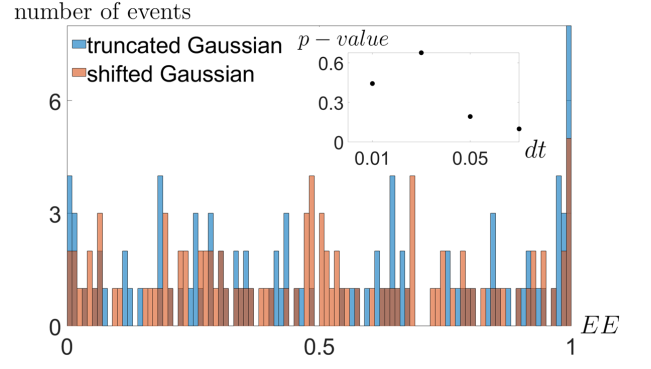


FIG. 11. Histogram of the steady state entanglement entropy distribution for various values of time increment in the numerics  $dt$ . Blue colour are data evolved using truncated Gaussian distribution at  $r_c$ , red colour uses (9). The parameters used for this histogram are  $b = 0.2, \gamma = 0.5$  and  $dt = 0.01$ . The inset shows  $p$ -values calculated for various  $dt$  using the Two-sample Kolmogorov-Smirnov test, revealing an upward trend for decreasing  $dt$ , implying more overlapping between the data. For the values of  $b$  and  $dt$  considered in the histogram, the null hypothesis cannot be rejected, and the two different sets of data are statistically indistinguishable.

changes some of the factor slightly for later convenience:

$$\begin{aligned} \hat{k}_j(x, \lambda) &= \mathcal{N}_j \exp\left(-\frac{(x - 2\lambda\hat{O}_j)^2}{4\Delta^2}\right) \\ \hat{k}_j(x, \lambda) |\psi_t\rangle &= \tilde{\mathcal{N}}_j \exp\left(-\frac{x^2}{4\Delta^2}\right) \exp\left(\frac{\lambda\hat{O}_j x}{\Delta^2}\right) |\psi_t\rangle \end{aligned} \quad (\text{B.1})$$

An initial normalised density matrix  $\rho_0$  is updated as

$$\frac{\hat{k}_j(x, \lambda)\rho_0\hat{k}_j^\dagger(x, \lambda)}{\text{Tr}[\hat{k}_j(x, \lambda)\rho_0\hat{k}_j^\dagger(x, \lambda)]} = \frac{\check{\rho}_{x,\lambda}}{\text{Tr}[\check{\rho}_{x,\lambda}]} \quad (\text{B.2})$$

The average density matrix  $\bar{\rho}$  across all measurement outcome at a particular time step is

$$\begin{aligned} \bar{\rho} &= \int_{-\infty}^{\infty} dx \frac{\check{\rho}_{x,\lambda}}{\text{Tr}[\check{\rho}_{x,\lambda}]} P(x, \lambda) \\ \bar{\rho} &= \int_{-\infty}^{\infty} dx \hat{k}_j(x, \lambda)\rho_0\hat{k}_j^\dagger(x, \lambda) \\ &= \tilde{\mathcal{N}}_j^2 \int_{-\infty}^{\infty} dx \exp\left(-\frac{x^2}{2\Delta^2}\right) \exp\left(\frac{x\lambda\hat{O}_j}{\Delta^2}\right) \rho_0 \exp\left(\frac{x\lambda\hat{O}_j}{\Delta^2}\right) \end{aligned} \quad (\text{B.3})$$

which implies

$$\begin{aligned} \int_{-\infty}^{\infty} dx \hat{k}_j^\dagger(x, \lambda)\hat{k}_j(x, \lambda) &= \mathbb{I} \\ \tilde{\mathcal{N}}_j^2 \int_{-\infty}^{\infty} dx \exp\left(-\frac{x^2}{2\Delta^2}\right) \exp\left(\frac{x\lambda\hat{O}_j}{\Delta^2}\right) &= \mathbb{I} \end{aligned} \quad (\text{B.4})$$

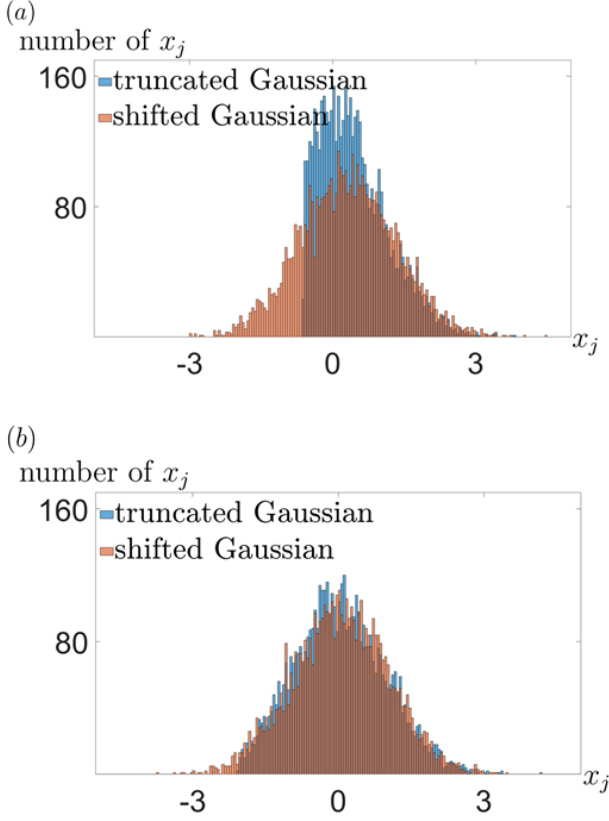


FIG. 12. Histograms of the truncated Gaussian  $P_{rc}(x_j)$  and shifted Gaussian  $\underline{P}(x_j)$  in (6). (a): samplings drawn from the truncated Gaussian (blue) and the shifted Gaussian (red) for  $dt = 0.05$ , and the null hypothesis is rejected at a significance level of 0.05. The p-value from KS2 sample test is 0.00. (b): similar to (a) but samples generated with  $dt = 0.001$ . The p-value is 0.31 and the null hypothesis cannot be rejected, indicating the distribution is statistically indistinguishable. The values of the parameters used here are  $\langle O_j \rangle = 1, b = 1$  and  $\gamma = 0.5$  and we used 5000 samplings of the distributions.

Rewriting

$$\Delta^2 = \Delta'^2 \lambda / \delta t, x = M_j \Delta'^2 \text{ and } \gamma = \lambda / \Delta'^2 = \lambda^2 / \Delta'^2 \delta t \quad (\text{B.5})$$

(B.4) becomes

$$\tilde{N}_j^2 \int_{-\infty}^{\infty} dM_j \exp\left(-\frac{M_j^2 \delta t}{2\gamma}\right) \exp\left(2M_j \hat{O}_j \delta t\right) = \mathbb{I} \quad (\text{B.6})$$

and one can interpret that the Kraus operator is alternatively described by

$$\begin{aligned} \bar{k}(M_j) &= \exp\left(M_j \hat{O}_j \delta t\right) \\ \int_{-\infty}^{\infty} d\mu(M_j) \bar{k}^\dagger(M_j) \bar{k}(M_j) &= \mathbb{I} \end{aligned} \quad (\text{B.7})$$

and normalised over the Gaussian measure  $d\mu(M_j) \propto dM_j \exp\left(-\frac{M_j^2 \delta t}{2\gamma}\right)$ , which describes a Gaussian random

variable  $M_j$  with mean  $\mathbb{E}_G[M_j] = 0$  and variance  $\mathbb{E}_G[M_j^2] = \gamma / \delta t$ .

The readout of a continuous measurement is now represented by the variable  $M_j$ , and its backaction on the system is given by the Kraus operator in (B.7). To generalise it to a time process, we first give  $M_j(t_l)$  a time index  $t_l = l\delta t$ . Then, an initial density matrix  $\rho_0$  evolves from time  $t_0 = 0$  to  $t_N = T = N\delta t$  as

$$\check{\rho}_M(T) = \prod_{l=1}^{l=N} \bar{k}(M_j(t_l)) \rho(0) \bar{k}^\dagger(M_j(t_l)), \quad (\text{B.8})$$

where  $M$  labels the quantum trajectory. In the time continuum limit, (B.8) becomes

$$\begin{aligned} \check{\rho}_M &= K(t) \rho(0) K^\dagger(t) \\ K(t) &= \exp\left[-i \int_0^T dt' H(t')\right] = \exp\left[-i \int_0^T dt' iM_j(t') \hat{O}_j\right] \end{aligned} \quad (\text{B.9})$$

and  $\mathbb{E}_G[M_j(t)] = 0$ ,  $\mathbb{E}_G[M_j(t)M_j(t')] = \gamma\delta(t-t')$ . From (B.9), we observe that the overall effect of a continuous measurement generates a random non-Hermitian Hamiltonian  $H(t) = iM_j(t)\hat{O}_j$  in time. Generalisation to multiple measurement  $j = 1 \dots L$ , and including another competing set, follows the same line as each process is independent to each other, and we arrive at Eq.(33) in the main text.

In the case of PPS, we saw, in Appendix A, that PPS shifts the mean of the random variable  $x$  by  $\delta\lambda$ . We can interpret this as a shift in the mean of the measure. Using the relationship Eq.(B.5), Eq.(7), and setting  $\gamma = 1$  as an overall energy scale

$$\begin{aligned} d\mu(M_j) &\xrightarrow{PPS} dx \exp\left(-\frac{(x - \delta\lambda)^2}{2\Delta^2}\right) \\ &\propto dM_j \exp\left(-\frac{(M_j - \frac{1-\zeta}{\zeta}\gamma)^2 \delta t}{2\gamma}\right), \end{aligned} \quad (\text{B.10})$$

we arrive at Eq.(19) where the mean of the Gaussian average is shifted by  $\mathbb{E}_G[M_j] = 1 - \zeta$ , as required from PPS. The generalisation to multiple weak continuous measurements is straightforward, with different measurements corresponding to different non-Hermitian noises, and taking the time continuum limit yields Eq.(21) (since noises from different measurements are independent of each other, cross product between different noise vanishes in time continuum limit).

### Appendix C: operator-state correspondence and replica majorana Hamiltonian

In this appendix and below, we distinguish the ket or bra space in the Choi–Jamiolkowski isomorphism by  $\sigma = \pm$  to replace  $\uparrow$  and  $\downarrow$  in the main text.

The Choi–Jamiołkowski isomorphism maps an operator to a duplicated Hilbert space:

$$\hat{O} = \sum_{i,j} O_{i,j} |i\rangle \langle j| \xrightarrow{\text{Choi}} \sum_{i,j} O_{i,j} |i\rangle \otimes |j\rangle = |\hat{O}\rangle \quad (\text{C.1})$$

Under Choi–Jamiołkowski isomorphism, the trace operation between 2 operators becomes a transition amplitude:

$$\text{Tr}[\hat{A}^\dagger \hat{B}] \xrightarrow{\text{Choi}} \langle \hat{A} | \hat{B} \rangle \quad (\text{C.2})$$

hence equ (24). When dealing with density matrix  $\rho$ , the action of some operator on the density matrix becomes action on the Choi state:

$$\begin{aligned} \hat{A}\rho &= \sum_{i,j,k} A_{i,j} \rho_{j,k} |i\rangle \langle k| \xrightarrow{\text{Choi}} \sum_{i,j,k} A_{i,j} \rho_{j,k} |i\rangle |k\rangle = \hat{A} \otimes \mathbb{I} |\rho\rangle \\ \rho \hat{A} &\xrightarrow{\text{Choi}} \mathbb{I} \otimes \hat{A}^T |\rho\rangle, \quad \hat{B}\rho \hat{A} \xrightarrow{\text{Choi}} \hat{B} \otimes \hat{A}^T |\rho\rangle \end{aligned} \quad (\text{C.3})$$

and hence (22). Writing out explicitly the average dynamics of  $n$ -replica described by (23):

$$\begin{aligned} &\mathbb{E}_G^{(PPS)} [(K(t) \otimes K^*(t))^{\otimes n} |\rho^{(n)}(0)\rangle] \\ &= \mathbb{E}_G^{(PPS)} \left[ \exp \left( -i \int_0^t H_n(t') dt' \right) \right] |\rho^{(n)}(0)\rangle \\ H_n(t) &= \sum_{\substack{\sigma=\pm \\ a=1,\dots,n}} \sum_j [J_j(t') + i\sigma M_j(t')] i\chi_j^{(\sigma a)} \chi_{j+1}^{(\sigma a)} \end{aligned} \quad (\text{C.4})$$

where  $\sigma$  distinguish ket/bra space,  $a$  for replica:  $\chi_j^{(\downarrow a)} = \mathbb{I}^{\otimes 2a+1} \otimes \chi_j^* \otimes \mathbb{I}^{\otimes 2a}$ ,  $\chi_j^{(\uparrow a)} = \mathbb{I}^{\otimes 2a} \otimes \chi_j \otimes \mathbb{I}^{\otimes 2a+1}$ . Up to this point, the Majorana operator  $\chi_j^{(\sigma a)}$  is not well defined as they anti-commute within the same branch and replica while commuting each other in different branches or replicas. To resolve this, one should first map the

fermionic Hilbert space to a spin-1/2 Hilbert space, then define new Majorana operators which differ from the one in (C.4) by a Klein factor, which is essentially a Pauli string in the replica space [18]. More precisely, let us first define a Pauli string across a single replica (for simplicity, we implicitly assume  $L$  to be a multiple of 4):

$$F^{(\sigma a)} = \prod_{j=1}^{j=L} \chi_j^{(\sigma a)}, \quad (\text{C.5})$$

which is equivalent to the total parity of replica  $\sigma a$ . Then, the following anti-commuting real fermionic operator can be constructed:

$$\begin{aligned} \chi_j'^{(\uparrow a)} &= \prod_{a'=1}^{a'<a} [F^{(\uparrow a')} F^{(\downarrow a')}] \chi_j^{(\uparrow a)} \\ \chi_j'^{(\downarrow a)} &= \prod_{a'=1}^{a'<a} [F^{(\uparrow a')} F^{(\downarrow a')}] F^{(\uparrow a)} \chi_j^{(\downarrow a)}. \end{aligned} \quad (\text{C.6})$$

It can be checked that these newly defined Majorana operators anti-commute in the duplicated replica Hilbert space i.e.  $\{\chi_j'^{(\sigma a)}, \chi_l'^{(\sigma' a')}\} = \delta_{j,l} \delta_{\sigma,\sigma'} \delta_{a,a'}$ . Moreover, bilinear products of the form  $\chi_j^{(\sigma a)} \chi_{j+1}^{(\sigma a)}$  is unchanged:  $\chi_j^{(\sigma a)} \chi_{j+1}^{(\sigma a)} = \chi_j'^{(\sigma a)} \chi_{j+1}'^{(\sigma a)}$ . To lighten the notation, we simply denote these proper replica Majorana operators as  $\chi_j^{(\sigma a)}$ , as we make no use of the original ill-behaved Majorana operators.

To evaluate (C.4), we expand it using cumulant expansion up to 2nd order  $\langle e^A \rangle \approx \exp[\langle A \rangle + 1/2(\langle A^2 \rangle - \langle A \rangle^2)]$  and note that the Gaussian measure now centred at  $(1-\zeta)\Xi_j$ . With a slight abuse of notation by calling the new anti-commuting Majorana as  $\chi_j'^{(\sigma a)} \rightarrow \chi_j^{(\sigma a)}$ , for  $n=2$  we arrive at (37).

Finally, the boundary state  $|\mathcal{C}_{2,\mathbf{A}}\rangle, |\mathbb{I}\rangle$  have the following properties with the Pauli matrices in the replica space  $\sigma_{\alpha,j}^{(a)}$ ,  $\alpha = x, y, z$   $a = 1, 2$  [18]:

$$\begin{aligned} \sigma_{\alpha,j}^{(a)} \mathbb{I} \sigma_{\alpha,j}^{(a)} &= \mathbb{I} \xrightarrow{\text{Choi}} i\chi_j^{(+a)} \chi_j^{(-a)} |\mathbb{I}\rangle = |\mathbb{I}\rangle \\ \sigma_{\alpha,j}^{(a)} \mathcal{C}_{2,\mathbf{A}} \sigma_{\alpha,j}^{(a)} &= \mathcal{C}_{2,\mathbf{A}} \xrightarrow{\text{Choi}} i\chi_j^{(+a)} \chi_j^{(-a)} |\mathcal{C}_{2,\mathbf{A}}\rangle = |\mathcal{C}_{2,\mathbf{A}}\rangle, \quad j \notin \mathbf{A} \\ \sigma_{\alpha,j}^{(2)} \mathcal{C}_{2,\mathbf{A}} \sigma_{\alpha,j}^{(1)} &= \mathcal{C}_{2,\mathbf{A}} \xrightarrow{\text{Choi}} -i\chi_j^{(+2)} \chi_j^{(-1)} |\mathcal{C}_{2,\mathbf{A}}\rangle = |\mathcal{C}_{2,\mathbf{A}}\rangle, \quad j \in \mathbf{A} \\ \sigma_{\alpha,j}^{(1)} \mathcal{C}_{2,\mathbf{A}} \sigma_{\alpha,j}^{(2)} &= \mathcal{C}_{2,\mathbf{A}} \xrightarrow{\text{Choi}} i\chi_j^{(+1)} \chi_j^{(-2)} |\mathcal{C}_{2,\mathbf{A}}\rangle = |\mathcal{C}_{2,\mathbf{A}}\rangle, \quad j \in \mathbf{A} \end{aligned} \quad (\text{C.7})$$

#### Appendix D: Solution for 2-replica for monitored case

Recall that the effective Hamiltonian without PPS reads

$$\mathcal{H} = \frac{1}{2} \sum_j J^2 \left( \sum_{\substack{\sigma=\pm \\ a=1,2}} i\chi_j^{(\sigma a)} \chi_{j+1}^{(\sigma a)} \right)^2 - \gamma_j \left( \sum_{\substack{\sigma=\pm \\ a=1,2}} \sigma i\chi_j^{(\sigma a)} \chi_{j+1}^{(\sigma a)} \right)^2 \quad (\text{D.1})$$

one can write it entirely as local SO(4) generators defined using Majorana operators:

$$S_j^{\alpha,\beta} = \frac{i}{2} [\chi_j^\alpha, \chi_j^\beta] \quad (\text{D.2})$$

and for generic  $J^2, \gamma$ , only a subset of (D.2) commutes with  $\mathcal{H}$  [18, 66]. An important set of local symmetry which will become clear are the local on-site parity  $\mathcal{R}_j = \prod_a i\gamma^{(+a)}\gamma^{(-a)}, [\mathcal{R}_j, \mathcal{H}] = 0$ .

One can readily define the following spin-1/2 operators:

$$\Sigma^\mu = \frac{1}{2} \mathbf{c}_j^\dagger \sigma_\mu \mathbf{c}_j \quad (\text{D.3})$$

where  $\sigma_\alpha, \alpha = x, y, z$  are the usual Pauli matrices and  $\mathbf{c}_j = (c_{j,\uparrow}, c_{j,\downarrow})^T$ . The other spin-1/2 generators is associated with the  $\eta$  spin in the Hubbard model, generated via Shiba transformation [82, 93].

$$\eta_j^z = \frac{1}{2} (c_{j,\uparrow}^\dagger c_{j,\uparrow} + c_{j,\downarrow}^\dagger c_{j,\downarrow} - 1), \quad \eta_j^+ = c_{j,\uparrow}^\dagger c_{j,\downarrow}^\dagger \quad (\text{D.4})$$

these two species of SU(2) generators stems from the fact that  $\text{SO}(4) \cong [\text{SU}(2) \times \text{SU}(2)]/\mathbb{Z}_2$ . The quotient by  $\mathbb{Z}_2$  comes from the criterion that

$$\sum_j [\eta_j^z + \Sigma_j^z] = \sum_j c_{j,\uparrow}^\dagger c_{j,\uparrow} - \frac{L}{2} \in \mathbb{Z} \quad (\text{D.5})$$

and  $\eta_j^z, \Sigma_j^z$  can either be both integer or both half-integer (assuming  $L$  is even). Recalling that the local parity operator  $\mathcal{R}_j = \pm 1$  commutes with  $\mathcal{H}$ , constructing the projector  $\Pi_{j,+} = \frac{1}{2} (1 + \mathcal{R}_j)$  we observe that

$$\Pi_{j,+} \Sigma_j^\mu \Pi_{j,+} = 0, \quad \text{while } \Pi_{j,+} \eta_j^\mu \Pi_{j,+} = \eta_j^\mu \quad (\text{D.6})$$

hence the two different SU(2)  $\Sigma^\mu, \eta^\mu$  acts on  $\mathcal{R}_j = \mp 1$  sector respectively. The choice of the initial state  $|\rho(0)\rangle = |\mathbb{I}\rangle, \mathcal{R}_j |\mathbb{I}\rangle = +1 |\mathbb{I}\rangle$  fixes the sector and should match the sector the boundary state is in. To complete the prove that  $\eta^\mu$  (and hence  $\Sigma^\mu$ ) are spin-1/2 operators, we demonstrate that the total spin operator has eigenvalue:

$$\eta_j^{x2} + \eta_j^{y2} + \eta_j^{z2} |\mathbb{I}\rangle = \frac{4}{3} |\mathbb{I}\rangle = S(1+S) |\mathbb{I}\rangle \quad (\text{D.7})$$

where  $S = 1/2$ .

The SO(4) generators in (D.2) can be expressed in term of these two SU(2) generators i.e.  $S^{+1,+2} = 2(\Sigma^z + \eta^z)$ . Writing (D.1) in terms of (D.4) and (D.3), we arrive at (43) and the physics can readily be extracted via usual means i.e. Bethe Ansatz and bosonisation.

### Appendix E: effective spin Hamiltonian and bosonisation details

As mentioned in the main text, there are two conserved charges  $[\sum_j \gamma_j^{(\sigma 1)} \gamma_j^{(\sigma 2)}, \mathcal{H}]$ , which suggest the following

2 complex fermions:

$$c_{j,\uparrow}^\dagger = \frac{\gamma_j^{(+1)} + i\gamma_j^{(+2)}}{2}, \quad c_{j,\downarrow}^\dagger = \frac{\gamma_j^{(-1)} - i\gamma_j^{(-2)}}{2} \quad (\text{E.1})$$

Written in terms of the complex fermions, it becomes  $[\mathcal{H}, N_\sigma] = 0, N_\sigma = \sum_j c_{j,\sigma}^\dagger c_{j,\sigma}, \sigma = \uparrow, \downarrow$ . These two conserved  $U(1)$  charges will be the basis for abelian bosonisation later. Inserting this relationship and followed by an unitary transformation  $c_{j,\uparrow}^\dagger \rightarrow (i)^j c_{j,\uparrow}^\dagger, c_{j,\downarrow}^\dagger \rightarrow (-i)^j c_{j,\downarrow}^\dagger$ , the Majorana operators are transformed as:

$$\begin{aligned} -i(\gamma_j^{(+1)}\gamma_{j+1}^{(+1)} + \gamma_j^{(+2)}\gamma_{j+1}^{(+2)}) &\rightarrow -2(c_{j,\uparrow}^\dagger c_{j+1,\uparrow} + c_{j+1,\uparrow}^\dagger c_{j,\uparrow}) \\ i(\gamma_j^{(-1)}\gamma_{j+1}^{(-1)} + \gamma_j^{(-2)}\gamma_{j+1}^{(-2)}) &\rightarrow -2(c_{j,\downarrow}^\dagger c_{j+1,\downarrow} + c_{j+1,\downarrow}^\dagger c_{j,\downarrow}) \end{aligned} \quad (\text{E.2})$$

Inserting these into (37), we arrive at (40).

We now proceed to bosonise (40) w.r.t. the basis  $\sigma = \uparrow, \downarrow$ . We first compute terms corresponding to no dimerisation  $\mathcal{O}(\Delta)^0$ .  $H_0$  the kinetic part gives the usual free Luttinger liquid Hamiltonian with  $K = 1$ :

$$H_0 = \frac{v_F}{2\pi} \sum_{\sigma=\uparrow,\downarrow} \int_x (\partial_x \theta_\sigma)^2 + (\partial_x \phi_\sigma)^2 \quad (\text{E.3})$$

With bosonisation, we can investigate the strong PPS limit where  $J^2, \gamma \ll B$ . This is the limit at which the excitation is small compare to the Fermi energy and bosonisation remains valid. As bosonising a lattice model will inevitably generate term whose appearance depends directly on the filling fraction, the filling fraction is determined by utilising the properties in (C.7) which gives

$$\begin{aligned} \langle\langle \mathbb{I} | i\chi_j^{(+1)} \chi_j^{(-2)} | \mathbb{I} \rangle\rangle &= 0 \\ \langle\langle \mathbb{I} | -\chi_j^{(+1)} \chi_j^{(+2)} | \mathbb{I} \rangle\rangle &= 0 \\ \langle\langle \mathbb{I} | (c_{j,\uparrow}^\dagger + c_{j,\uparrow}) (c_{j,\uparrow}^\dagger - c_{j,\uparrow}) | \mathbb{I} \rangle\rangle &= 0 \\ \langle\langle \mathbb{I} | 1 - 2c_{j,\uparrow}^\dagger c_{j,\uparrow} | \mathbb{I} \rangle\rangle &= 0 \end{aligned} \quad (\text{E.4})$$

similarly for  $c_{j,\downarrow}^\dagger$  and the boundary state  $|\mathcal{C}_{2,\mathbf{A}}\rangle$ . Therefore, this specifies that we are dealing with half filling  $k_F = \pi/2$  and some term that oscillates with  $e^{4ik_F x}$  should in fact be kept.

The term  $H_{umk}$  in (40) becomes

$$\begin{aligned} H_{umk} &\propto \sum_{\sigma=\uparrow,\downarrow} (c_{j,\sigma}^\dagger c_{j+1,\sigma} + c_{j+1,\sigma}^\dagger c_{j,\sigma})^2 \\ &= -2 \sum_{\sigma=\uparrow,\downarrow} (c_{j,\sigma}^\dagger c_{j,\sigma} - \frac{1}{2}) (c_{j+1,\sigma}^\dagger c_{j+1,\sigma} - \frac{1}{2}) \\ &\approx -2a \sum_{\sigma=\uparrow,\downarrow} \int_x \frac{2}{\pi^2} (\partial_x \phi_\sigma)^2 - \frac{2}{(2\pi\alpha)^2} \cos 4\phi_\sigma \end{aligned} \quad (\text{E.5})$$

while  $H_m$  gives

$$\begin{aligned}
H_m &\propto \sum_j (c_{j,\uparrow}^\dagger c_{j+1,\uparrow} + h.c.) (c_{j,\downarrow}^\dagger c_{j+1,\downarrow} + h.c.) \\
&\approx a \int_x \left[ \frac{4}{2\pi} \nabla \phi_\uparrow + \frac{e^{2ik_F x}}{2\pi\alpha} 2ie^{-i2\phi_\uparrow(x)} - \frac{e^{-2ik_F x}}{2\pi\alpha} 2ie^{i2\phi_\uparrow(x)} \right] \\
&\quad \times \left[ \uparrow \rightarrow \downarrow \right] \\
&= a \int_x \frac{4}{\pi^2} \nabla \phi_\uparrow \nabla \phi_\downarrow + \frac{8}{(2\pi\alpha)^2} \cos[2(\phi_\uparrow - \phi_\downarrow)] \\
&\quad - \frac{8}{(2\pi\alpha)^2} \cos[2(\phi_\uparrow + \phi_\downarrow)] \tag{E.6}
\end{aligned}$$

The  $\cos 4\phi_\sigma$  is highly irrelevant under RG compare to the cosines from (E.6) and therefore can be discarded without much concerns.

We now move on to terms coming from dimerisation  $\mathcal{O}(\Delta)^1$ . This amounts to looking for  $e^{2ik_F x}$  components from bosonisation as  $(-1)^j = e^{2ik_F x}$ . Bosonising  $H_0$  gives the following term

$$\begin{aligned}
&-2(1-\zeta)\Delta \sum_{\eta=\uparrow,\downarrow}^j (-1)^j (c_{j+1,\eta}^\dagger c_{j,\eta} + h.c.) \\
&\approx \frac{16a(1-\zeta)\Delta\pi}{(2\pi\alpha)^2} \sum_{\eta=\uparrow,\downarrow} \int_x \sin 2\phi_\eta \tag{E.7}
\end{aligned}$$

which is highly relevant.  $H_{umk}$  requires some attention and bosonisation should be treated carefully within fermion normal ordering  $\underline{\psi(x)_R \psi^\dagger(x')_R} = [2\pi(x-x')]^{-1}$ ,  $\underline{\psi(x)_L \psi^\dagger(x')_L} = -[2\pi(x-x')]^{-1}$  [94].

In the end, this give  $H_{umk}$  the following term

$$\begin{aligned}
&-4\zeta\Delta \sum_{\eta=\uparrow,\downarrow}^j (-1)^j (c_{j,\eta}^\dagger c_{j,\eta} - \frac{1}{2})(c_{j+1,\eta}^\dagger c_{j+1,\eta} - \frac{1}{2}) \\
&= \frac{-16a\zeta\Delta}{(2\pi\alpha)^2} \sum_{\eta=\uparrow,\downarrow} \int_x \sin 2\phi_\eta(x) \tag{E.8}
\end{aligned}$$

and a less relevant operator  $(\partial_x \phi)^2 \sin 2\phi$  have been discarded. For  $H_m$ , the  $2k_F$  component gives terms  $\nabla \phi_\uparrow \cos 2\phi_\downarrow + \nabla \phi_\downarrow \cos 2\phi_\uparrow$  which is irrelevant in the current model: By power counting, it can be seen that its dimension is  $1 + \frac{K_\rho + K_\sigma}{2}$ . Since  $K_\rho, K_\sigma \geq 1$  from (47), this term is simply irrelevant in the current setting.

Inserting these results, and performing a unitary rotation to the charge and spin degree of freedom  $\phi_\rho = \frac{\phi_\uparrow + \phi_\downarrow}{\sqrt{2}}$ ,  $\phi_\sigma = \frac{\phi_\uparrow - \phi_\downarrow}{\sqrt{2}}$ , we arrive at (46).

## Appendix F: Boundary state $|\mathcal{C}_{2,\mathbf{A}}\rangle$

In this appendix, we discuss the state  $|\mathcal{C}_{2,\mathbf{A}}\rangle$  (the fundamental object in the computation of  $S_{2,\mathbf{A}}^{(cond)}$ ) and its expression in various bases. Our discussion is an extension to Ref. 66, which we contain here for self-consistency. For simplicity, we assume the region  $\mathbf{A}$  to be continuous.

To begin with, we note that  $|\mathcal{C}_{2,\mathbf{A}}\rangle$  belongs to the half-filling sector (cf appendix E), and there should exist some rotation between the two. More precisely, consider the identity operator before the Choi–Jamiolkowski isomorphism. In fermionic occupation basis, it can be expressed as:

$$\mathbb{I} = \frac{1}{2^{L/2}} \sum_{\vec{n}_1} |\vec{n}_1\rangle \langle \vec{n}_1|, \tag{F.1}$$

where  $\vec{n}_p$  is a string of length  $L/2$ , consists of either 0 or 1 i.e.  $\{0 \text{ or } 1\}^{\otimes L/2}$ .  $|\vec{n}_1\rangle$  can also be expressed as  $\prod_{j=1}^{j=L/2} (f_j^\dagger)^{n_{1,j}} |vac\rangle$ , where  $f_j^\dagger$  is a complex fermionic creation operator at site  $j$ , which can readily be defined from the Majorana operator in the model (cf Eq.(33)). In the duplicated 2-replica Hilbert space  $\mathcal{H} \otimes \mathcal{H}^* \otimes \mathcal{H} \otimes \mathcal{H}^*$ , the identity operator is mapped to a state  $|\mathbb{I}\rangle$  which appears as:

$$\begin{aligned}
|\mathbb{I}\rangle &= \frac{1}{2^L} \sum_{\vec{n}_1, \vec{n}_2} |\vec{n}_1, \vec{n}_1\rangle \otimes |\vec{n}_2, \vec{n}_2\rangle \\
&= \frac{1}{2^L} \sum_{\vec{n}_1, \vec{n}_2} \prod_j (f_j^{\dagger(\uparrow 1)})^{n_{1,j}} \prod_j (f_j^{\dagger(\downarrow 1)})^{n_{1,j}} \prod_j (f_j^{\dagger(\uparrow 2)})^{n_{2,j}} \prod_j (f_j^{\dagger(\downarrow 2)})^{n_{2,j}} |vac\rangle \\
&= \frac{1}{2^L} \sum_{\vec{n}_1, \vec{n}_2} g(|\vec{n}_1|, |\vec{n}_2|) \prod_j (f_j^{\dagger(\uparrow 1)})^{n_{1,j}} (f_j^{\dagger(\downarrow 1)})^{n_{1,j}} (f_j^{\dagger(\uparrow 2)})^{n_{2,j}} (f_j^{\dagger(\downarrow 2)})^{n_{2,j}} |vac\rangle
\end{aligned}$$

$$\text{where } g(|\vec{n}_1|, |\vec{n}_2|) = (-1)^{\frac{|\vec{n}_1|}{2}(|\vec{n}_1|-1) + \frac{|\vec{n}_2|}{2}(|\vec{n}_2|-1)}, \text{ and } f_j^{\dagger(\sigma a)} = \frac{\chi_{2j-1}^{(\sigma a)} + i\chi_{2j}^{(\sigma a)}}{2} \quad (\text{F.2})$$

$g(|\vec{n}_1|, |\vec{n}_2|)$  is a factor accounting for the transformation from the replica-local basis (line 2) to site-local basis (line 3). Under the Choi–Jamiolkowski isomorphism mapping, the operator  $\mathcal{C}_{2,\mathbf{A}}$  (cf Eq.(14)) is mapped to

$$\begin{aligned}
|\mathcal{C}_{2,\mathbf{A}}\rangle &= \frac{1}{2^L} \sum_{\vec{n}_1, \vec{n}_2} |\vec{n}_1\rangle |\vec{n}_{2,\mathbf{A}}, \vec{n}_{1\bar{\mathbf{A}}}\rangle \otimes |\vec{n}_2\rangle |\vec{n}_{1\mathbf{A}}, \vec{n}_{2\bar{\mathbf{A}}}\rangle \\
&= \frac{1}{2^L} \sum_{\vec{n}_1, \vec{n}_2} g(|\vec{n}_1|, |\vec{n}_2|) \bigotimes_{j \in \mathbf{A}} |n_{1,j}, n_{2,j}\rangle \otimes |n_{2,j}, n_{1,j}\rangle \bigotimes_{j \in \bar{\mathbf{A}}} |n_{1,j}, n_{1,j}\rangle \otimes |n_{2,j}, n_{2,j}\rangle \\
&= \prod_{j \in \mathbf{A}} \hat{\mathcal{C}}_{2,j} |\mathbb{I}\rangle,
\end{aligned} \quad (\text{F.3})$$

where  $\vec{n}_{i,\mathbf{A}}$  denotes the string of  $\vec{n}_i$  in region  $\mathbf{A}$  (similarly for its compliment  $\bar{\mathbf{A}}$ ). Expressed in site-local basis, one observes that  $|\mathcal{C}_{2,\mathbf{A}}\rangle$  is merely a rotation on  $|\mathbb{I}\rangle$  which can be implemented by a site-local operator

$$\hat{\mathcal{C}}_{2,j} = f_j^{\dagger(\downarrow 1)} f_j^{(\downarrow 2)} + f_j^{(\downarrow 1)} f_j^{\dagger(\downarrow 2)} + \frac{1}{2}(1 + \Pi_{j,\downarrow 1} \Pi_{j,\downarrow 2}), \quad (\text{F.4})$$

where  $\Pi_{j,\sigma a} = 1 - 2f_j^{\dagger(\sigma a)} f_j^{(\sigma a)}$ . Utilising

$$\begin{aligned}
\sum_{l=0,1} \left( c_{2j+l,\downarrow}^\dagger c_{2j+l,\downarrow} - \frac{1}{2} \right) &= i(f_j^{\dagger(\downarrow 1)} f_j^{(\downarrow 2)} + f_j^{(\downarrow 1)} f_j^{\dagger(\downarrow 2)}) \\
- \left[ \sum_{l=0,1} \left( c_{2j+l,\downarrow}^\dagger c_{2j+l,\downarrow} - \frac{1}{2} \right) \right]^2 &= \frac{1}{2}(1 + \Pi_{j,\downarrow 1} \Pi_{j,\downarrow 2}) - 1,
\end{aligned} \quad (\text{F.5})$$

and after some manipulation, we arrive at (cf Eq.(41))

$$\begin{aligned}
\hat{\mathcal{C}}_{2,j} &= e^{-i\frac{\pi}{2} \sum_{l=0,1} (c_{2j+l,\downarrow}^\dagger c_{2j+l,\downarrow} - \frac{1}{2})} \\
\prod_j \hat{\mathcal{C}}_{2,j} &= \exp \left[ -i\frac{\pi}{2} \sum_{m=m_l}^{m=m_r} \left( c_{m,\downarrow}^\dagger c_{m,\downarrow} - \frac{1}{2} \right) \right].
\end{aligned} \quad (\text{F.6})$$

In the last line, we denote the left (right) boundary of region  $\mathbf{A}$  by  $m = m_l$  ( $m = m_r$ ). Note that there are  $2L$   $c$ -fermions and  $L$   $f$ -fermions. Eq.(F.6) can readily be bosonised by keeping only the slowest oscillating terms and note that we are at half-filling (cf Eq.(E.4)). This leads to [69]

$$\begin{aligned}
c_{m,\downarrow}^\dagger c_{m,\downarrow} &\approx -\frac{1}{\pi} \partial_x \phi_\downarrow(x_m) + \rho_0 \\
\prod_j \hat{\mathcal{C}}_{2,j} &\approx \exp \left[ i\frac{1}{2} (\phi_\downarrow(x_r) - \phi_\downarrow(x_l)) \right],
\end{aligned} \quad (\text{F.7})$$

and Eq.(52) follows. To justify the replacement of the state  $|\mathbb{I}\rangle$  by the ground state of  $\mathcal{H}$ ,  $|\text{GS}\rangle$ , we note that both the state  $|\mathbb{I}\rangle$  and  $|\text{GS}\rangle$  belongs to the half-filling sector and therefore their overlap is finite. The state  $|\mathbb{I}\rangle$  is  $U(1)$  symmetry breaking in both  $\uparrow$  and  $\downarrow$  sector [66]. This amounts to picking out a  $\theta$  field configuration in both sector in the bosonised language, while leaving the  $\phi$  configuration unaffected. Since we are interested in the computation of the  $\phi$  field correlation, such replacement only amounts to an unimportant constant proportional to the overlap  $\langle\langle \mathbb{I} | \text{GS} \rangle\rangle$ , which is subsystem size independent. This concludes the proof of Eq.(52).

### Appendix G: RG flow for Sine-Gordon Hamiltonian

The procedure here is a real space renormalisation group procedure that follows closely with Ref. 69 and 86. We will also demonstrate explicitly that the umklapp term  $H_{\text{umk}}$  in (40) is way less relevant. The form of Sine-Gordon Hamiltonian we encounter from Umklapp term and dimerisation has the following form

$$H = \sum_{i=1,2} \frac{1}{2\pi} \int dx u_i K_i (\partial_x \theta_i)^2 + \frac{u_i}{K_i} (\partial_x \phi_i)^2 + \frac{2g}{(2\pi\alpha)^2} \int dx \cos(\beta\phi_1) \cos(\beta\phi_2) \quad (\text{G.1})$$

where  $K_i, u_i$  are the Luttinger parameter and velocity of two different bosonic field species  $\phi_i, \theta_i$ .  $\beta$  is the frequency and it is  $\sqrt{8}$  for the umklapp term while  $\sqrt{2}$  for dimerisation term. To begin with, consider the following correlation function

$$R(r_1 - r_2) = \langle e^{ia^2\sqrt{2}\phi_1(r_1)} e^{-ia^2\sqrt{2}\phi_1(r_2)} \rangle_H \quad (\text{G.2})$$

The average with respect to the free kinetic part of the Hamiltonian  $H_0 = \sum_{i=1,2} \frac{1}{2\pi} \int dx u_i K_i (\partial_x \theta_i)^2 + \frac{u_i}{K_i} (\partial_x \phi_i)^2$  is

$$\langle e^{ia^2\sqrt{2}\phi_i(r_1)} e^{-ia^2\sqrt{2}\phi_i(r_2)} \rangle_{H_0} = e^{-a^2 K_i F_{1,i}(r_1 - r_2)} \simeq \left( \frac{\alpha}{r_1 - r_2} \right)^{a^2 K_i} \\ \langle [\phi(r_1) - \phi(r_2)]^2 \rangle_{H_0} = K_i F_{1,i}(r_1 - r_2), \quad F_{1,i}(r) = \frac{1}{2} \log \left[ \frac{x^2 + (u_i|\tau| + \alpha)^2}{\alpha^2} \right] \quad (\text{G.3})$$

Since the Hamiltonian is separable in the kinetic part, averages w.r.t. to the free kinetic Hamiltonian can be performed separably  $\langle f(\phi_1)g(\phi_2) \rangle_{H_0} = \langle f(\phi_1) \rangle_{H_{0,1}} \langle g(\phi_2) \rangle_{H_{0,2}}$ . The full action reads:

$$S = \overbrace{\sum_{i=1,2} \frac{1}{2\pi K_i} \int dx d\tau \frac{1}{u_i} (\partial_\tau \phi)^2 + u_i (\partial_x \phi)^2}^{S_{0,1} + S_{0,2}} + \frac{2g}{(2\pi\alpha)^2} \int dx d\tau \cos(\beta\phi_1) \cos(\beta\phi_2) \quad (\text{G.4})$$

$\theta$  has been integrated out as it merely contributes a constant which cancels out in the expectation value. As  $u_1 \neq u_2$ , there is an extra non-trivial factor towards the end. If we expand in powers of  $g$  the first order is 0 and stopping at second order, the partition function is

$$Z = \int \mathcal{D}\phi_1 \mathcal{D}\phi_2 e^{-S} \\ = \int \mathcal{D}\phi_1 \mathcal{D}\phi_2 e^{-S_{0,1} - S_{0,2}} \left[ 1 - 0 + \frac{1}{32} \left( \frac{2g}{(2\pi\alpha)^2} \right)^2 \int d^2 r' d^2 r'' \prod_{i=1,2} \sum_{\epsilon_1, \epsilon_2 = \pm} e^{i\epsilon_1 \beta \phi_i(r')} e^{-i\epsilon_2 \beta \phi_i(r'')} \right] \quad (\text{G.5})$$

$d^2 r = dx d\tau$  is different to the conventional definition for now. Expanding G.2 in  $g$  and stopping at 2nd order, we have

$$\langle e^{ia^2\sqrt{2}\phi_1(r_1)} e^{-ia^2\sqrt{2}\phi_1(r_2)} \rangle_H \approx e^{-a^2 K_1 F_{1,1}(r_1 - r_2)} \\ + \frac{1}{8} \left( \frac{g}{(2\pi\alpha)^2} \right)^2 \left[ \int d^2 r' d^2 r'' \langle e^{ia^2\sqrt{2}\phi_1(r_1)} e^{-ia^2\sqrt{2}\phi_1(r_2)} \prod_{i=1,2} \sum_{\epsilon_1, \epsilon_2 = \pm} e^{i\epsilon_1 \beta \phi_i(r')} e^{-i\epsilon_2 \beta \phi_i(r'')} \rangle_{H_0} \right. \\ \left. - e^{-a^2 K_1 F_{1,1}(r_1 - r_2)} \langle \prod_{i=1,2} \sum_{\epsilon_1, \epsilon_2 = \pm} e^{i\epsilon_1 \beta \phi_i(r')} e^{-i\epsilon_2 \beta \phi_i(r'')} \rangle_{H_0} \right] \\ = e^{-a^2 K_1 F_{1,1}(r_1 - r_2)} \left[ 1 + \frac{1}{8} \left( \frac{g}{(2\pi\alpha)^2 u_1} \right)^2 \int d^2 r' d^2 r'' e^{-\frac{\beta^2}{2} (K_1 F_{1,1}(r' - r'') + K_2 F_{1,2}(r' - r''))} \right. \\ \left. \times 2 \sum_{\epsilon = \pm} \left( e^{\frac{\alpha\beta}{\sqrt{2}} K_1 \epsilon [F_{1,1}(r_1 - r') - F_{1,1}(r_1 - r'') + F_{1,1}(r_2 - r') - F_{1,1}(r_2 - r'')]} - 1 \right) \right], \quad y = u_1 \tau \quad (\text{G.6})$$

Due to factor  $e^{-\frac{\beta^2}{2}K_1F_{1,1}(r'-r'')} \sim (\frac{1}{r'})^{\frac{\beta^2}{2}}$  which is a power law, only small  $r' - r''$  contributes the most. Making

$$\begin{aligned} R &= \frac{r' + r''}{2}, \quad r = r' - r'' \\ r_1 - r' &= r_1 - R - \frac{1}{2}r, \quad r_1 - r'' = r_1 - R + \frac{1}{2}r \end{aligned} \quad (\text{G.7})$$

We can expand in  $r$  giving

$$\begin{aligned} &\sum_{\epsilon=\pm} e^{\frac{\alpha\beta}{\sqrt{2}}K_1\epsilon[F_{1,1}(r_1-r')-F_{1,1}(r_1-r'')+F_{1,1}(r_2-r'')-F_{1,1}(r_2-r')]} - 1 \\ &\approx \frac{a^2\beta^2}{2}K_1^2 \left[ \sum_{i,j=x,y} r_i \nabla_{R_j} (F_{1,1}(r_1 - R) - F_{1,1}(r_2 - R)) \right]^2 \end{aligned} \quad (\text{G.8})$$

the integral is only non-zero for  $i = j$  ( $i \neq j$  odd function) and  $\int d^2rx^2 = \int d^2ry^2 = \int d^2r\frac{r^2}{2}$ . With integration by part [G.6](#) becomes,

$$\begin{aligned} &= e^{-a^2K_1F_{1,1}(r_1-r_2)} \left[ 1 - \frac{1}{16} \left( \frac{g}{(2\pi\alpha)^2u_1} \right)^2 \int d^2rd^2R e^{-\frac{\beta^2}{2}(K_1F_{1,1}(r)+K_2F_{1,2}(r))} \right. \\ &\quad \left. \times a^2\beta^2K_1^2r^2 [F_{1,1}(r_1 - R) - F_{1,1}(r_2 - R)] (\nabla_X^2 + \nabla_Y^2) [F_{1,1}(r_1 - R) - F_{1,1}(r_2 - R)] \right] \end{aligned} \quad (\text{G.9})$$

Since  $F_{1,1}(r) \simeq \log(\frac{r}{\alpha})$  for  $r > \alpha$ , we can use the following identity

$$(\nabla_X^2 + \nabla_Y^2) \log(R) = 2\pi\delta(R) \quad (\text{G.10})$$

and  $\int d^2R [F_{1,1}(r_1 - R) - F_{1,1}(r_2 - R)] (\nabla_X^2 + \nabla_Y^2) [F_{1,1}(r_1 - R) - F_{1,1}(r_2 - R)] = -4\pi F_{1,1}(r_1 - r_2)$ .  $F_{1,1}(0) = 0$  with regularisation. At this point we need to remember that

$$F_{1,2}(r) = \log \left[ \frac{\sqrt{x^2 + (\frac{u_2}{u_1}|y| + \alpha)^2}}{\alpha} \right] \simeq \log \left[ \frac{\sqrt{x^2 + (\frac{u_2}{u_1}|y|)^2}}{\alpha} \right] = \log \left[ \frac{r\sqrt{1 + \epsilon_1\cos^2(\theta)}}{\alpha} \right] \quad (\text{G.11})$$

$(\frac{u_2}{u_1})^2 = 1 + \epsilon_1$ , and the above behaviour for  $F_{1,2}$  approximately holds true provided  $\epsilon > -1$  (regularisation can be appropriately ignored). [G.2](#) is thus

$$\begin{aligned} R(r_1 - r_2) &\approx e^{-a^2K_1F_{1,1}(r_1-r_2)} \left[ 1 + F_{1,1}(r_1 - r_2) \frac{a^2\beta^2K_1^2\pi}{4} \left( \frac{g}{(2\pi\alpha)^2u_1} \right)^2 \int_{r>\alpha} d^2r e^{-\frac{\beta^2}{2}(K_1F_{1,1}(r)+K_2F_{1,2}(r))} r^2 \right] \\ &= e^{-a^2K_1F_{1,1}(r_1-r_2)} \left[ 1 + F_{1,1}(r_1 - r_2) \frac{a^2\beta^2K_1^2}{2\pi} \frac{g^2}{32\pi^2\alpha^4u_1^2} \int_{\alpha}^{\infty} r^3 dr \int_{-\pi}^{\pi} d\theta \left( \frac{\alpha}{r} \right)^{\frac{\beta^2}{2}(K_1+K_2)} \left( \frac{1}{1 + \epsilon_1\cos\theta} \right)^{\frac{\beta^2K_2}{4}} \right] \\ &= e^{-a^2K_1F_{1,1}(r_1-r_2)} \left[ 1 + F_{1,1}(r_1 - r_2) \frac{a^2\beta^2K_1^2}{32} \frac{\tilde{g}^2 I(\epsilon_1, K_2, \beta)}{2\pi} \int_{\alpha}^{\infty} \left( \frac{\alpha}{r} \right)^{\frac{\beta^2}{2}(K_1+K_2)-3} \frac{dr}{\alpha} \right] \end{aligned} \quad (\text{G.12})$$

$\tilde{g} = \frac{g}{\pi u_1}, I(\epsilon_1, K_2, \beta) = \int_{-\pi}^{\pi} d\theta \left( \frac{1}{1 + \epsilon_1\cos\theta} \right)^{\frac{\beta^2K_2}{4}}$ . The bracket can be re-exponentiated giving.

$$K_{1,eff}(\alpha) = K_1 - \frac{g(\alpha)^2\beta^2K_1^2}{32\pi^2u_1^2} \frac{I(\epsilon_1, K_2, \beta)}{2\pi} \int_{\alpha}^{\infty} \left( \frac{\alpha}{r} \right)^{\frac{\beta^2}{2}(K_1+K_2)-3} \frac{dr}{\alpha} \quad (\text{G.13})$$

If we change the cutoff  $\alpha = \alpha' + d\alpha$  and re-parametrise  $\alpha = \alpha_0 e^l$ ,  $K_{1,eff}$  and  $g$  has to change accordingly giving the renormalisation group flow shown below. The flow for  $K_2$  can be worked out with the same procedure but replacing

$\phi_1 \rightarrow \phi_2$  in the correlator  $\langle e^{ia^2\sqrt{2}\phi_i(r_1)} e^{-ia^2\sqrt{2}\phi_i(r_2)} \rangle_{H_0}$ . All in all, we have

$$\begin{aligned}\partial_l K_1 &= -\frac{g^2\beta^2 K_1^2}{32\pi^2 u_1^2} \frac{I(\epsilon_1, K_2, \beta)}{2\pi} \\ \partial_l K_2 &= -\frac{g^2\beta^2 K_2^2}{32\pi^2 u_2^2} \frac{I(\epsilon_2, K_1, \beta)}{2\pi} \\ \partial_l g &= \left(2 - \frac{\beta^2}{4}(K_1 + K_2)\right)g\end{aligned}\tag{G.14}$$

$\epsilon_2 = -\frac{\epsilon_1}{1+\epsilon_1}$ . With this we can immediately tell the Umklapp term  $\beta = \sqrt{8}$  is simply less relevant while for dimerisation  $\beta = \sqrt{2}$  is highly relevant.

The RG flow for usual Sine-Gordon Hamiltonian of the form  $H = \frac{1}{2\pi} \int dx uK(\partial_x\theta)^2 + \frac{u}{K}(\partial_x\phi)^2 + \frac{2g}{(2\pi\alpha)^2} \int dx \cos(\beta\phi)$  can be worked out similarly and the extra factor  $I(\epsilon_1, K_2, \beta)$  reduces to 1.

## Appendix H: Details about numerics

The procedures for our numerics employed follow the steps described in Ref. 10, which is an extension of Ref. 13 to generic particle non-conserving case. Across all simulations, the length of the associated complex fermion chain is set to a multiple of 4 and we employ open boundary condition in order to compute a meaningful topological entanglement entropy. The discrete-time parameter  $\delta t$  has been chosen to be 0.05, and the number of trajectories for each set of parameters is typically above 600.

To simulate the PPS dynamics, we employ (9), assuming inhomogeneous measurement strength, and since the measurement operators  $\hat{O}_j$ 's square to  $\mathbb{I}$ , it reduces to

$$\begin{aligned}d|\psi_t\rangle &= \frac{1}{N} \left[ (-iH - \sum_j \zeta \Xi_j \hat{O}_j \langle \hat{O}_j \rangle + \sum_j (1-\zeta) \Xi_j \hat{O}_j) dt \right. \\ &\quad \left. + \sum_j dW_j \hat{O}_j \right] |\psi_t\rangle\end{aligned}\tag{H.1}$$

where  $N$  is some normalisation,  $dW_j dW'_j = \zeta \Xi_j dt \delta_{j,j'}$  is the Wiener process, and we have absorbed any operator-independent term into the normalisation. One can exponentialise this expression, which gives

$$\begin{aligned}|\psi_{t+dt}\rangle &= \frac{1}{N_1} \exp \left[ -iHdt - dt \sum_j \zeta \Xi_j \hat{O}_j \langle \hat{O}_j \rangle \right. \\ &\quad \left. + dt(1-\zeta) \sum_j \Xi_j \hat{O}_j + \sum_j dW_j \hat{O}_j \right] |\psi_t\rangle\end{aligned}\tag{H.2}$$

$H$  is a white noise with homogeneous strength and shares the same set of operators  $\hat{O}_j$  with the measurement. The overall evolution is explicitly written as

$$\begin{aligned}|\psi_{t+dt}\rangle &= \frac{1}{N_1} \exp \left[ -i \sum_j \hat{O}_j d\xi_j - dt \sum_j \zeta \Xi_j \hat{O}_j \langle \hat{O}_j \rangle \right. \\ &\quad \left. + dt(1-\zeta) \sum_j \Xi_j \hat{O}_j + \sum_j dW_j \hat{O}_j \right] |\psi_t\rangle\end{aligned}\tag{H.3}$$

where  $d\xi_j d\xi_{j'} = J^2 \delta_{j,j'} dt$ ,  $d\xi_j dW_{j'} = 0$  is another Wiener process. In the case of deterministic unitary, one can trotterise the update into measurement and unitary separately

$$|\psi_{t+\delta t}\rangle = \frac{1}{N} e^{-iH\delta t} e^{-\delta t \sum_j \zeta \Xi_j \hat{O}_j \langle \hat{O}_j \rangle + \delta t(1-\zeta) \sum_j \Xi_j \hat{O}_j + \sum_j \delta W_j \hat{O}_j} |\psi_t\rangle$$

where  $\delta t$  is the discrete time interval and  $\delta W_j$ 's are random variables with mean 0 and variance  $\gamma\delta t$ . In the lowest order of error, it is merely  $[H\delta t, \delta W_j \hat{O}_j] \sim \mathcal{O}(\delta t^{3/2})$  which vanishes as  $\delta t$  is reduced. (H.3) however includes white noises as unitary update and lowest order of error becomes  $\mathcal{O}(\delta t)$  which does not vanishes in the time continuum limit. Therefore, the safest route is to not trotterise the update into measurement and unitary blocks, and instead retain them in a single exponential while discretising time with  $\delta t$ ,  $\delta W_j$  and  $\delta \xi_j$  (mean 0 and variance  $J^2\delta t$ ). We have numerically check that this does have a slight effect on the outcome of the simulation.

To simulate the Majorana chain, we implement the calculate in the Bogoliubov de Gennes (BdG) formalism, by first identifying 1 species of complex fermion to rewrite the chain:  $c_j^\dagger = (\chi_{2j-1} + i\chi_{2j})/2$ . The operators of interest, which are the odd and even bond parity, become the on-site and cross-site parity:

$$\begin{aligned}i\chi_{2j-1}\chi_{2j} &= (1 - 2c_j^\dagger c_j) \\ i\chi_{2j}\chi_{2j+1} &= (c_j^\dagger - c_j)(c_{j+1}^\dagger + c_{j+1})\end{aligned}\tag{H.4}$$

As the model including the measurement is Gaussian preserving, starting from a Gaussian state, the evolution will remain in the space of Gaussian states. For a generic Gaussian state, one can express it as [10, 95]

$$|\psi\rangle = \prod_{n=1}^{n=L} \sum_{k,n} V_{k,n}^* c_k^\dagger + U_{k,n}^* c_k\tag{H.5}$$

where  $V$  and  $U$  are  $L \times L$  matrices which form a  $2L \times 2L$  orthonormal matrix

$$W = \begin{pmatrix} U & V^* \\ V & U^* \end{pmatrix}\tag{H.6}$$

and implies  $U^\dagger U + V^\dagger V = \mathbb{I}$ ,  $U^T V + V^T U = 0$ . Any Gaussian state is fully characterised by the set of all two point correlators; All two point correlation can be calculated from directly from  $V$  and  $U$  as

$$\begin{aligned} C_{i,j} &= \langle c_i^\dagger c_j \rangle = V^* V^T \\ F_{i,j} &= \langle c_i c_j \rangle = V * U^T \end{aligned} \quad (\text{H.7})$$

Therefore, it is enough to evolve the matrices  $U$  and  $V$  alone. To achieve this, the white noise and measurement are written in the basis of complex fermion shown in (H.4) giving 2 separate non-commuting set of white noise and measurement. In the BdG formalism, each set of noise/measurement is represented by a matrix:

$$\begin{aligned} \sum_j (1 - 2c_j^\dagger c_j) &\equiv \underline{c}^\dagger M_{2j-1} \underline{c} \\ \sum_j (c_j^\dagger - c_j)(c_{j+1}^\dagger + c_{j+1}) &\equiv \underline{c}^\dagger M_{2j} \underline{c} \end{aligned} \quad (\text{H.8})$$

where  $\underline{c} = (c_1^\dagger, c_2^\dagger, \dots, c_L^\dagger, c_1, \dots, c_L)^T$ , and the matrices are

$$\begin{aligned} M_{2j-1} &= 2\mathbb{I}_{L \times L} \\ M_{2j} &= \begin{pmatrix} -A & B^\dagger \\ B & A \end{pmatrix} \\ A &= \text{diag}(1, 1) + \text{diag}(1, -1), B = -\text{diag}(1, 1) + \text{diag}(1, -1) \end{aligned} \quad (\text{H.9})$$

$\text{diag}(1, \pm 1)$  indicate 1 along the  $\pm 1$  off diagonal. Dimerisation implemented in the original Majorana chain corresponds to grouping the measurement strengths into two sets  $\{\zeta \Xi_{2j-1}\} = \gamma$ ,  $\{\zeta \Xi_{2j}\} = \alpha$ , each with uniform strength within them (and hence  $(1 - \zeta)\Xi_j$  into  $(1 - \zeta)_\gamma, (1 - \zeta)_\alpha$ ) and the ratio gives the dimerisation  $\frac{1-\Delta}{1+\Delta} = \frac{\gamma}{\alpha}$ . Denoting  $(1 - 2c_j^\dagger c_j) = \hat{\Gamma}_j$  and  $(c_j^\dagger - c_j)(c_{j+1}^\dagger + c_{j+1}) = \hat{A}_j$ , (H.3) becomes

$$\begin{aligned} \frac{1}{N} \exp \left[ -i \sum_j \hat{\Gamma}_j d\xi_{1,j} - i \sum_j \hat{A}_j d\xi_{2,j} - \gamma dt \sum_j \hat{\Gamma}_j \langle \hat{\Gamma}_j \rangle - \alpha dt \sum_j \hat{A}_j \langle \hat{A}_j \rangle + (1 - \zeta)_\gamma dt \sum_j \hat{\Gamma}_j + (1 - \zeta)_\alpha \sum_j \hat{A}_j \right. \\ \left. + \sum_j \hat{\Gamma}_j dW_{\gamma,j} + \sum_j \hat{A}_j dW_{\alpha,j} \right] \end{aligned} \quad (\text{H.10})$$

$d\xi_{k,j} d\xi_{l,j'} = J^2 dt \delta_{j,j'} \delta_{k,l}$ ,  $dW_{\gamma,j} dW_{\gamma,j'} = \gamma dt \delta_{j,j'}$  and  $dW_{\alpha,j} dW_{\alpha,j'} = \alpha dt \delta_{j,j'}$ . The update of the matrices  $V$  and  $U$  can now be implemented in the BdG form, and in the first step, they are multiplied by:

$$\begin{pmatrix} \tilde{U}(t + \delta t) \\ \tilde{V}(t + \delta t) \end{pmatrix} = \exp[M] \begin{pmatrix} \tilde{U}(t) \\ \tilde{V}(t) \end{pmatrix} \quad (\text{H.11})$$

where  $M$ , a matrix, is merely the exponential in (H.10) written in BdG form, and the operators are replaced by matrices of the form in (H.9) where entries are appropriately multiplied by the random variables  $\delta\xi_{k,j}$ ,  $\delta W_{\gamma,j}$  and  $\delta W_{\alpha,j}$ . The expectation values present can readily be computed from two point correlators in and (H.7). As  $\tilde{U}$  and  $\tilde{V}$  does not meet the criterion below (H.6), a final step involves a normalisation of the state to ensure  $W$  is orthonormal, which can be implemented via any orthonormalisation procedure of a matrix: QR, Gram-Schmidt or singular value decomposition. Here, we chose QR and the final update is

$$QR = \begin{pmatrix} \tilde{U}(t + \delta t) \\ \tilde{V}(t + \delta t) \end{pmatrix}, \begin{pmatrix} U(t + \delta t) \\ V(t + \delta t) \end{pmatrix} = Q \quad (\text{H.12})$$

$U(t + \delta t)$  and  $V(t + \delta t)$  are now properly normalised.

To compute the entanglement entropy, recall that the

Nambu one-body Green's function matrix is

$$G = \begin{pmatrix} \mathbb{I}_{L \times L} - C^T & F \\ F^\dagger & C \end{pmatrix} \quad (\text{H.13})$$

The entanglement entropy of a subsystem  $\mathbf{A}$  is calculated by reducing the Green's function to only fermions operators in  $\mathbf{A}$ ,  $G_{\mathbf{A}}$ , and is given by [96]

$$S_{1,\mathbf{A}} = - \sum_{\{\lambda_j\}} [\lambda_j \log_2 \lambda_j + (1 - \lambda_j) \log_2 \lambda_j] \quad (\text{H.14})$$

where  $\{\lambda_j\}$  are the set of eigenvalues of  $G_{\mathbf{A}}$ . For completeness, higher order entropies are

$$S_{n,\mathbf{A}} = \frac{1}{1-n} \sum_{\{\lambda_j\}} \log_2 [(\lambda_j)^n + (1 - \lambda_j)^n] \quad (\text{H.15})$$

To extract the critical exponent  $\nu$  in the measurement-only scenario, a finite-size scaling analysis on the topological entanglement entropy ( $S_{TEE}$ ) is performed [10, 39, 87, 88]. In 1D systems, it is computed via [97]

$$S_{TEE} = S_{AB} + S_{BC} - S_B - S_{ABC}, \quad (\text{H.16})$$

where the partitions  $A$ ,  $B$  and  $C$  are pictured in fig. 13. We fix the on-site parity measurement strength to some

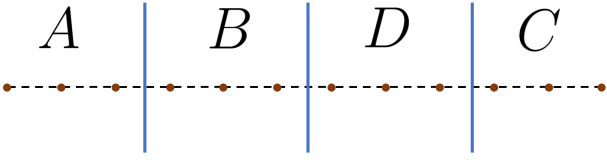


FIG. 13. Partition of the system for topological entanglement entropy calculation. The blue lines divide the system into 4 equal partitions.

value  $\gamma = \gamma_0$  for numerical convenience and vary  $\alpha$  (equivalent to varying  $\Delta$ ).

As the choice of the parameter for finite-scaling analysis cannot be made arbitrarily, we justify as follows:  $S_{TEE}$  (in log base 2) has a definite value of 0 (1), in the thermodynamic limit, in the topologically trivial (non-trivial) area-law phase i.e. it is a step function across the phase transition. This can be heuristically understood based on the fact that the two area law phases are characterised by the dominant measurements of Majorana odd or even bond parity, which destroy (odd) or retain (even) long-range entanglement between the 2 Majorana fermions at the opposite edges. With the properties discussed above, we note that  $S_{TEE}$  is a valid order parameter between the two different phases and displays singular behaviour at the phase transition in the thermodynamic limit. In a finite system, although the crossing (the singular behaviour of a step) is smeared out, the crossing point is scale-invariant: due to the emergent conformal invariance at the critical point, the length-dependence of the different terms in Eq.(H.16) cancels each other out. We can further elaborate on this and derive a suitable ansatz (the discussion here follows closely to that in Ref. 89): using the fact that  $S_{TEE}$  is scale-invariant at the critical point (giving a crossing point across different system sizes) and it is dimensionless in length, an educated guess is

$$\begin{aligned} S_{TEE} &= G(\xi/L) = G((\alpha - \alpha_{crit})^{-\nu}/L) \\ &= F((\alpha - \alpha_{crit})L^{\frac{1}{\nu}}), \end{aligned} \quad (\text{H.17})$$

where  $\xi$ , the correlation length, diverges at the critical point and  $F(x)$  is some well-behaved function at  $x = 0$ . In the second equality, we use the fact that  $\xi \sim (\alpha - \alpha_{crit})^{-\nu}$  in a quantum phase transition (where the parameter  $\alpha$  plays the role of temperature in thermal transition). This justifies the use and the choice of  $S_{TEE}$ .

We note that it is also possible to use the connected 2-point correlation function to extract the exponent  $\nu$ . However, in practice, this is not the optimal method since this quantity is heavily affected by the finite size effect and  $\xi$  often becomes larger than the system sizes one can access.

In the thermodynamic limit, the critical point is located at  $\alpha_{crit} = \gamma_0$ .  $S_{TEE}$  is computed for various system sizes  $L$  at a given  $\zeta$  across an interval of  $\alpha$  in the vicinity of  $\alpha = \gamma_0$ . Using the scaling form in Eq.(H.17) ( $F$  is some unknown function),  $S_{TEE}$  for various system

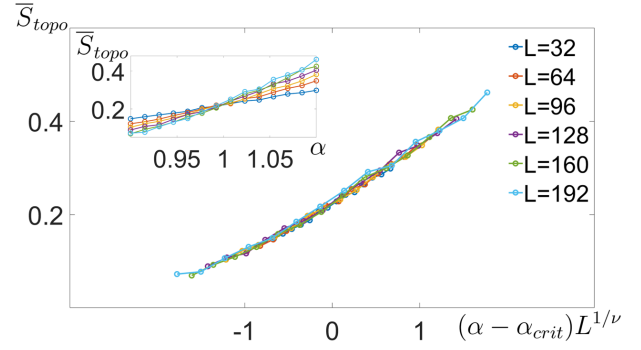


FIG. 14. Example of data collapse of the topological entanglement entropy using the scaling form in Eq. (H.17). The parameters used are  $\gamma_0 = 1, \alpha_{crit} = 1, \gamma/B = 1.82$ . The value  $\nu = 1.83$  is obtained from the best-fit procedure. Inset: Raw data for the topological entanglement entropy against  $\alpha$ . before finite size scaling collapse.

sizes will collapse onto a single curve around the critical point (see Fig. 14) for some suitable value of  $\alpha_{crit}$  and  $\nu$  [10, 34, 89]. The true critical point,  $\alpha_{crit}$ , can be read off from the crossing point of  $S_{TEE}$  from different  $L$ 's as shown in the inset of Fig. 14, and is generally found to be  $\gamma_0 \pm 2\%$  (it can be further located using the optimizing function below). One notable exception is  $\zeta = 0.4$  which appears to deviate more than 2% from  $\gamma_0$  ( $\gamma_0 = 1, \alpha_{crit, \zeta=0.4} = 0.975$ ); however, it is still within the 5% error range.

For the data collapse,  $\nu$  is used as a fitting parameter, and its value is determined by the ‘best’ data collapse which is quantified by the following objective function [34]:

$$\begin{aligned} \epsilon(\nu) &= \sum_{i=2}^{n-1} (y_i - \bar{y}_i)^2 \\ \text{where } \bar{y}_i &= \frac{(x_{i+1} - x_i)y_{i-1} - (x_{i-1} - x_i)y_{i+1}}{x_{i+1} - x_{i-1}} \end{aligned} \quad (\text{H.18})$$

$x_i$  are defined to be  $(\alpha_i - \alpha_{crit})L^{1/\nu}$  and  $y_i = S_{TEE}(\alpha_i, L_i)$ .  $i$  labels different data points and their ordering is sorted based on ascending order in  $x'_i$ :  $x_1 < x_2 < \dots < x_n$ . The ‘best’ data collapse corresponds to the minimum of  $\epsilon(\nu)$ , at a given  $\alpha_{crit}$ , and we follow the convention in [34, 39] to define the error as the range of  $\nu$  which falls within 2 times the minimum  $\epsilon(\nu) < 2\epsilon(\nu)_{min}$ . In addition,  $\alpha_{crit}$  is further narrowed down by locating the global minimum of  $\epsilon(\nu)$ , accounting for  $\alpha_{crit}$  as well.

As a final point, to distinguish clearly numerically  $(\log L)^2$  from  $(\log L)$ , one may employ the difference [18]

$$\delta S_{0,L} = S_{0,2L} - S_{0,L} \quad (\text{H.19})$$

where  $S_{0,L}$  is the half-system entanglement entropy. The subleading term are therefore cancelled in  $\delta S_{0,L}$ , and the

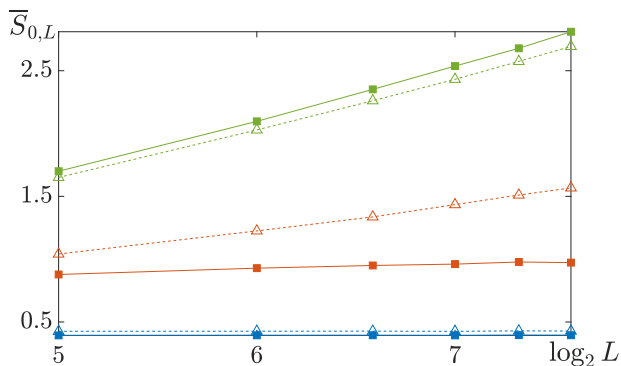


FIG. 15. Average half-cut entanglement entropy  $\bar{S}_{0,L}$  from numerical simulations illustrating the area law (blue markers/orange squares) and system-size-dependent entanglement scaling (green markers/orange triangles) phases for non-zero dimerization. The two sets of lines are  $\zeta = 0.091$  (filled squares/solid line) and  $\zeta = 0.2$  (hollow triangles/dashed lines), and different colour schemes represent different  $J^2$  values:  $J^2 = 0.09$  (blue),  $J^2 = 0.68$  (orange) and  $J^2 = 1.25$  (green). It should be noted that although the line  $\zeta = 0.091$ ,  $J^2 = 0.68$  (filled orange/solid) appears to be increasing for small  $L$ , this is likely to be a finite size effect as it is trending to saturation for larger  $L$ .

scaling are different:

$$\delta S_{0,L} \propto \begin{cases} \log_2 L, & \text{if } S_{0,L} \sim (\log \frac{L}{2})^2 \\ \text{constant}, & \text{if } S_{0,L} \sim \log \frac{L}{2} \end{cases} \quad (\text{H.20})$$

Fig. 15 reports the scaling of the half-cut entanglement entropy with system size. Increasing  $J^2$  for fixed  $\zeta = 0.091$  changes the scaling from area-law (full blue and orange squares) to system-size-dependent (full green squares). For  $\zeta = 0.2$ , the transition from the area-law (blue triangle) to size-dependent scaling (orange and green triangle) occurs at a smaller value of  $J^2$ . This is consistent with the theoretical finding from the bosonized theory in Fig. 9. Note that the exact value of the phase boundary is different from the one predicted within the 2-replica approximation, which is only expected to capture the qualitative behaviour, with a bias in favour of the area law phase [98].

- 
- [1] B. Skinner, J. Ruhman, and A. Nahum, Measurement-induced phase transitions in the dynamics of entanglement, *Physical Review X* **9**, 031009 (2019).
- [2] A. Chan, R. M. Nandkishore, M. Pretko, and G. Smith, Unitary-projective entanglement dynamics, *Physical Review B* **99**, 224307 (2019).
- [3] Y. Li, X. Chen, and M. P. Fisher, Quantum zeno effect and the many-body entanglement transition, *Physical Review B* **98**, 205136 (2018).
- [4] M. Szyniszewski, A. Romito, and H. Schomerus, Entanglement transition from variable-strength weak measurements, *Physical Review B* **100**, 064204 (2019).
- [5] M. P. Fisher, V. Khemani, A. Nahum, and S. Vijay, Random quantum circuits, *Annual Review of Condensed Matter Physics* **14**, 335 (2023).
- [6] J. M. Koh, S.-N. Sun, M. Motta, and A. J. Minnich, Measurement-induced entanglement phase transition on a superconducting quantum processor with mid-circuit readout, *Nature Physics* **19**, 1314–1319 (2023).
- [7] I. Google Quantum, A and Collaborators, Measurement-induced entanglement and teleportation on a noisy quantum processor, *Nature* **622**, 481–486 (2023).
- [8] C. Noel, P. Niroula, D. Zhu, A. Risinger, L. Egan, D. Biswas, M. Cetina, A. V. Gorshkov, M. J. Gullans, D. A. Huse, *et al.*, Measurement-induced quantum phases realized in a trapped-ion quantum computer, *Nature Physics* **18**, 760 (2022).
- [9] I. Poboiko, P. Pöpperl, I. V. Gornyi, and A. D. Mirlin, Theory of free fermions under random projective measurements, arXiv preprint arXiv:2304.03138 (2023).
- [10] G. Kells, D. Meidan, and A. Romito, Topological transitions in weakly monitored free fermions, *SciPost Physics* **14**, 031 (2023).
- [11] C. Carisch, A. Romito, and O. Zeitler, Quantifying measurement-induced quantum-to-classical crossover using an open-system entanglement measure, arXiv preprint arXiv:2304.02965 (2023).
- [12] M. Coppola, E. Tirrito, D. Karevski, and M. Collura, Growth of entanglement entropy under local projective measurements, *Physical Review B* **105**, 094303 (2022).
- [13] X. Cao, A. Tilloy, and A. De Luca, Entanglement in a fermion chain under continuous monitoring, *SciPost Physics* **7**, 024 (2019).
- [14] O. Alberton, M. Buchhold, and S. Diehl, Entanglement transition in a monitored free-fermion chain: From extended criticality to area law, *Physical Review Letters* **126**, 170602 (2021).
- [15] M. Buchhold, Y. Minoguchi, A. Altland, and S. Diehl, Effective theory for the measurement-induced phase transition of dirac fermions, *Physical Review X* **11**, 041004 (2021).
- [16] K. Yamamoto and R. Hamazaki, Localization properties in disordered quantum many-body dynamics under continuous measurement, *Physical Review B* **107**, L220201 (2023).
- [17] M. Szyniszewski, O. Lunt, and A. Pal, Disordered monitored free fermions, arXiv preprint arXiv:2211.02534 (2022).
- [18] M. Fava, L. Piroli, T. Swann, D. Bernard, and A. Nahum, Nonlinear sigma models for monitored dynamics of free fermions, arXiv preprint arXiv:2302.12820 (2023).
- [19] X. Turkeschi, L. Piroli, and M. Schiró, Enhanced entanglement negativity in boundary-driven monitored fermionic chains, *Physical Review B* **106**, 024304 (2022).
- [20] K. Chahine and M. Buchhold, Entanglement phases, localization and multifractality of monitored free fermions

- in two dimensions, arXiv preprint arXiv:2309.12391 (2023).
- [21] E. V. Doggen, Y. Gefen, I. V. Gornyi, A. D. Mirlin, and D. G. Polyakov, Generalized quantum measurements with matrix product states: Entanglement phase transition and clusterization, *Physical Review Research* **4**, 023146 (2022).
- [22] C.-M. Jian, H. Shapourian, B. Baue, and A. W. W. Ludwig, Measurement-induced entanglement transitions in quantum circuits of non-interacting fermions: Born-rule versus forced measurements, arXiv preprint arXiv:2302.09094 (2023).
- [23] B. Xing, X. Turkeshi, M. Schiró, R. Fazio, and D. Poletti, Interactions and integrability in weakly monitored hamiltonian systems, arXiv preprint arXiv:2308.09133 (2023).
- [24] Q. Tang and W. Zhu, Measurement-induced phase transition: A case study in the nonintegrable model by density-matrix renormalization group calculations, *Physical Review Research* **2**, 013022 (2020).
- [25] M. Buchhold, T. Mueller, and S. Diehl, Revealing measurement-induced phase transitions by pre-selection, arXiv preprint arXiv:2208.10506 (2022).
- [26] B. Ladewig, S. Diehl, and M. Buchhold, Monitored open fermion dynamics: Exploring the interplay of measurement, decoherence, and free hamiltonian evolution, *Physical Review Research* **4**, 033001 (2022).
- [27] Y. Minoguchi, P. Rabl, and M. Buchhold, Continuous gaussian measurements of the free boson CFT: A model for exactly solvable and detectable measurement-induced dynamics, *SciPost Phys.* **12**, 009 (2022).
- [28] T. Müller, S. Diehl, and M. Buchhold, Measurement-induced dark state phase transitions in long-ranged fermion systems, *Physical Review Letters* **128**, 010605 (2022).
- [29] T. Jin and D. G. Martin, Measurement-induced phase transition in a single-body tight-binding model, arXiv preprint arXiv:2309.15034 (2023).
- [30] C.-M. Jian, B. Bauer, A. Keselman, and A. W. Ludwig, Criticality and entanglement in nonunitary quantum circuits and tensor networks of noninteracting fermions, *Physical Review B* **106**, 134206 (2022).
- [31] P. Zhang, C. Liu, S.-K. Jian, and X. Chen, Universal entanglement transitions of free fermions with long-range non-unitary dynamics, *Quantum* **6**, 723 (2022).
- [32] T. Botzung, S. Diehl, and M. Müller, Engineered dissipation induced entanglement transition in quantum spin chains: From logarithmic growth to area law, *Physical Review B* **104**, 184422 (2021).
- [33] G. Giachetti and A. De Luca, Elusive phase transition in the replica limit of monitored systems, arXiv preprint arXiv:2306.12166 (2023).
- [34] A. Lavasani, Y. Alavirad, and M. Barkeshli, Topological order and criticality in  $(2+1)$  d monitored random quantum circuits, *Physical review letters* **127**, 235701 (2021).
- [35] S. Roy, J. Chalker, I. Gornyi, and Y. Gefen, Measurement-induced steering of quantum systems, *Physical Review Research* **2**, 033347 (2020).
- [36] D. Rossini and E. Vicari, Coherent and dissipative dynamics at quantum phase transitions, *Physics Reports* **936**, 1 (2021).
- [37] S. Sang and T. H. Hsieh, Measurement-protected quantum phases, *Physical Review Research* **3**, 023200 (2021).
- [38] M. Ippoliti, M. J. Gullans, S. Gopalakrishnan, D. A. Huse, and V. Khemani, Entanglement phase transitions in measurement-only dynamics, *Physical Review X* **11**, 011030 (2021).
- [39] A. Lavasani, Y. Alavirad, and M. Barkeshli, Measurement-induced topological entanglement transitions in symmetric random quantum circuits, *Nature Physics* **17**, 342 (2021).
- [40] L. Li, C. H. Lee, S. Mu, and J. Gong, Critical non-hermitian skin effect, *Nature communications* **11**, 5491 (2020).
- [41] K. Kawabata, T. Numasawa, and S. Ryu, Entanglement phase transition induced by the non-hermitian skin effect, *Physical Review X* **13**, 021007 (2023).
- [42] X. Turkeshi and M. Schiró, Entanglement and correlation spreading in non-hermitian spin chains, *Physical Review B* **107**, L020403 (2023).
- [43] S. Gopalakrishnan and M. J. Gullans, Entanglement and purification transitions in non-hermitian quantum mechanics, *Physical review letters* **126**, 170503 (2021).
- [44] R. Hamazaki, K. Kawabata, and M. Ueda, Non-hermitian many-body localization, *Physical review letters* **123**, 090603 (2019).
- [45] S. Mu, C. H. Lee, L. Li, and J. Gong, Emergent fermi surface in a many-body non-hermitian fermionic chain, *Physical Review B* **102**, 081115 (2020).
- [46] H.-G. Zirnstein, G. Refael, and B. Rosenow, Bulk-boundary correspondence for non-hermitian hamiltonians via green functions, *Physical review letters* **126**, 216407 (2021).
- [47] H.-G. Zirnstein and B. Rosenow, Exponentially growing bulk green functions as signature of nontrivial non-hermitian winding number in one dimension, *Physical Review B* **103**, 195157 (2021).
- [48] S. Malzard, C. Poli, and H. Schomerus, Topologically protected defect states in open photonic systems with non-hermitian charge-conjugation and parity-time symmetry, *Physical review letters* **115**, 200402 (2015).
- [49] L. Herviou, N. Regnault, and J. H. Bardarson, Entanglement spectrum and symmetries in non-hermitian fermionic non-interacting models, *SciPost Physics* **7**, 069 (2019).
- [50] D. Leykam, K. Y. Bliokh, C. Huang, Y. D. Chong, and F. Nori, Edge modes, degeneracies, and topological numbers in non-hermitian systems, *Physical review letters* **118**, 040401 (2017).
- [51] S. Yao and Z. Wang, Edge states and topological invariants of non-hermitian systems, *Physical review letters* **121**, 086803 (2018).
- [52] K. Jacobs, *Quantum measurement theory and its applications* (Cambridge University Press, 2014).
- [53] X. Turkeshi, A. Biella, R. Fazio, M. Dalmonte, and M. Schiró, Measurement-induced entanglement transitions in the quantum ising chain: From infinite to zero clicks, *Physical Review B* **103**, 224210 (2021).
- [54] Y. Le Gal, X. Turkeshi, and M. Schiró, Volume-to-area law entanglement transition in a non-hermitian free fermionic chain, *SciPost Physics* **14**, 138 (2023).
- [55] C. Zerba and A. Silva, Measurement phase transitions in the no-click limit as quantum phase transitions of a non-hermitean vacuum, arXiv preprint arXiv:2301.07383 (2023).
- [56] M. Stefanini and J. Marino, Orthogonality catastrophe beyond luttinger liquid from post-selection, arXiv preprint arXiv:2310.00039 (2023).
- [57] A. Paviglianiti, X. Turkeshi, M. Schiró, and A. Silva, En-

- hanced entanglement in the measurement-altered quantum ising chain, arXiv preprint arXiv:2310.02686 (2023).
- [58] X. Turkeshi, M. Dalmonte, R. Fazio, and M. Schirò, Entanglement transitions from stochastic resetting of non-hermitian quasiparticles, *Physical Review B* **105**, L241114 (2022).
- [59] X. Feng, S. Liu, S. Chen, and W. Guo, Absence of logarithmic and algebraic scaling entanglement phases due to the skin effect, *Physical Review B* **107**, 094309 (2023).
- [60] L. Su, A. Clerk, and I. Martin, Dynamics and phases of nonunitary floquet transverse-field ising model, arXiv preprint arXiv:2306.07428 (2023).
- [61] X. Chen, Y. Li, M. P. Fisher, and A. Lucas, Emergent conformal symmetry in nonunitary random dynamics of free fermions, *Physical Review Research* **2**, 033017 (2020).
- [62] Q. Tang, X. Chen, and W. Zhu, Quantum criticality in the nonunitary dynamics of  $(2+1)$ -dimensional free fermions, *Physical Review B* **103**, 174303 (2021).
- [63] S.-K. Jian, Z.-C. Yang, Z. Bi, and X. Chen, Yang-lee edge singularity triggered entanglement transition, *Physical Review B* **104**, L161107 (2021).
- [64] J. Despres, L. Mazza, and M. Schirò, Breakdown of linear spin-wave theory in a non-hermitian quantum spin chain, *Phys. Rev. B* **110**, 094304 (2024).
- [65] P. Sprent and N. C. Smeeton, *Applied nonparametric statistical methods* (CRC press, 2007).
- [66] Y. Bao, S. Choi, and E. Altman, Symmetry enriched phases of quantum circuits, *Annals of Physics* **435**, 168618 (2021).
- [67] Y. Bao, S. Choi, and E. Altman, Theory of the phase transition in random unitary circuits with measurements, *Physical Review B* **101**, 104301 (2020).
- [68] F. Evers and A. D. Mirlin, Anderson transitions, *Reviews of Modern Physics* **80**, 1355 (2008).
- [69] T. Giamarchi, *Quantum physics in one dimension*, Vol. 121 (Clarendon press, 2003).
- [70] A. Jamiolkowski, Linear transformations which preserve trace and positive semidefiniteness of operators, *Reports on Mathematical Physics* **3**, 275 (1972).
- [71] M.-D. Choi, Completely positive linear maps on complex matrices, *Linear algebra and its applications* **10**, 285 (1975).
- [72] This is equivalent to continuously measuring  $|01\rangle\langle 01|$  and/or  $|10\rangle\langle 10|$  independently since the two operators are not independent as a single particle occupies the system.
- [73] K. Snizhko, P. Kumar, and A. Romito, Quantum zeno effect appears in stages, *Phys. Rev. Res.* **2**, 033512 (2020).
- [74] P. Kumar, A. Romito, and K. Snizhko, Quantum zeno effect with partial measurement and noisy dynamics, *Physical Review Research* **2**, 043420 (2020).
- [75] A. Chantasri, J. Dressel, and A. N. Jordan, Action principle for continuous quantum measurement, *Physical Review A—Atomic, Molecular, and Optical Physics* **88**, 042110 (2013).
- [76] K. Koshino and A. Shimizu, Quantum zeno effect by general measurements, *Physics reports* **412**, 191 (2005).
- [77] S. A. Gurvitz, L. Fedichkin, D. Mozyrsky, and G. P. Berman, Relaxation and the zeno effect in qubit measurements, *Physical review letters* **91**, 066801 (2003).
- [78] C. Presilla, R. Onofrio, and U. Tambini, Measurement quantum mechanics and experiments on quantum zeno effect, *annals of physics* **248**, 95 (1996).
- [79] F. Li, J. Ren, and N. A. Sinitsyn, Quantum zeno effect as a topological phase transition in full counting statistics and spin noise spectroscopy, *Europhysics Letters* **105**, 27001 (2014).
- [80] For  $\zeta = 0$  and  $J > 1$  one can define a conditional 2-purity averaged over a time period. Such an average procedure would be immaterial if a steady-state solution exists.
- [81] Note that the percolation universality is specific of the model under consideration in the monitored projective limit.
- [82] C. N. Yang and S. Zhang, So 4 symmetry in a hubbard model, *Modern Physics Letters B* **4**, 759 (1990).
- [83] There is an implicit fermionic annihilation operator (Klein factor) at the front which commutes with all boson operator [69].
- [84] For a  $XXZ$ -spin 1/2 chain in the absence of magnetic field, bosonisation (without Bethe-ansatz) cannot capture the precise value of the phase boundary. Still, it distinguishes the XY phase from the anti-ferromagnetic/ferromagnetic Ising phase [69]. Here, bosonisation indicates a divergence of the Luttinger parameter at  $J_z/J_{xy} = -\pi/4 > -1$ , leading to the conclusion of a phase boundary separating the free Luttinger phase from a non-linear dispersing phase (in fact  $\omega \sim k^2$ ). While the location of the phase boundary predicted from bosonisation differs from the known phase boundary at  $J_z/J_{xy} = -1$ , the physics of the phase boundary from perturbation theory is correct Beyond its perturbative applicability.
- [85] D. Amit, Y. Goldschmidt, and S. Grinstein, Renormalisation group analysis of the phase transition in the 2d coulomb gas, sine-gordon theory and xy-model, *Journal of Physics A: Mathematical and General* **13**, 585 (1980).
- [86] J. V. José, L. P. Kadanoff, S. Kirkpatrick, and D. R. Nelson, Renormalization, vortices, and symmetry-breaking perturbations in the two-dimensional planar model, *Physical Review B* **16**, 1217 (1977).
- [87] K. Klocke and M. Buchhold, Topological order and entanglement dynamics in the measurement-only xxx quantum code, *Physical Review B* **106**, 104307 (2022).
- [88] K. Klocke and M. Buchhold, Majorana loop models for measurement-only quantum circuits, *Physical Review X* **13**, 041028 (2023).
- [89] A. W. Sandvik, Computational studies of quantum spin systems, in *AIP Conference Proceedings*, Vol. 1297 (American Institute of Physics, 2010) pp. 135–338.
- [90] D. B. Kaplan, J.-W. Lee, D. T. Son, and M. A. Stephanov, Conformality lost, *Physical Review D—Particles, Fields, Gravitation, and Cosmology* **80**, 125005 (2009).
- [91] Y. L. Gal, X. Turkeshi, and M. Schirò, Entanglement dynamics in monitored systems and the role of quantum jumps, arXiv preprint arXiv:2312.13419 (2023).
- [92] Y. Le Gal, X. Turkeshi, and M. Schirò, Entanglement dynamics in monitored systems and the role of quantum jumps, *PRX Quantum* **5**, 030329 (2024).
- [93] F. H. Essler, H. Frahm, F. Göhmann, A. Klümper, and V. E. Korepin, *The one-dimensional Hubbard model* (Cambridge University Press, 2005).
- [94] E. Orignac and T. Giamarchi, Weakly disordered spin ladders, *Physical Review B* **57**, 5812 (1998).
- [95] G. B. Mbeng, A. Russomanno, and G. E. Santoro, The quantum ising chain for beginners, arXiv preprint arXiv:2009.09208 **114** (2020).

- [96] V. Alba, M. Fagotti, and P. Calabrese, Entanglement entropy of excited states, *Journal of Statistical Mechanics: Theory and Experiment* **2009**, P10020 (2009).
- [97] B. Zeng and D.-L. Zhou, Topological and error-correcting properties for symmetry-protected topological order, *Europhysics Letters* **113**, 56001 (2016).
- [98] B. Ferte and X. Cao, Solvable model of quantum-darwinism-encoding transitions, *Physical Review Letters* **132**, 110201 (2024).
- [99] DOI to be added